



**Gold nanoparticles functionalised with fast water exchanging Gd<sup>3+</sup> chelates: linker effects on the relaxivity.**

Journal:	<i>Dalton Transactions</i>
Manuscript ID:	DT-ART-10-2014-003210.R2
Article Type:	Paper
Date Submitted by the Author:	29-Dec-2014
Complete List of Authors:	<p>Martins, Jos<math>\diamond</math>; University of Minho, Chemistry  Ferreira, Miguel; University of Minho, Chemistry  Ferreira, Paula; University of Minho, Chemistry  Gonçalves, Janaina; University of Minho, Chemistry  Geraldes, Carlos; UNIV. OF COIMBRA, Life Sciences;  Prata, Maria; University of Coimbra, IBILI,  Rodrigues, Sergio; University of Coimbra, Chemistry  Helm, Lothar; Ecole polytechnique federale de Lausanne, Institut des sciences et ingenierie chimiques  Mousavib, Bibimaryam; Laboratoire de Chimie Inorganique et Bioinorganique, Ecole Polytechnique Fédérale de Lausanne  Rodrigues, Tiago; Univerity of Cambridge, Biochemistry  Lopez-Larrubia, Pilar; CSIC, Instituto de Investigaciones Biomedicas  Cerdan, Sebastian; Instituto de Investigaciones Biomedicas , CSIC  Calle, Daniel; CSIC, Instituto de Investigaciones Biomedicas,</p>

1 **Gold Nanoparticles Functionalised with Fast Water Exchanging Gd<sup>3+</sup> Chelates:**  
2 **Linker Effects on the Relaxivity**

3  
4 Miguel F. Ferreira,<sup>a</sup> Janaina Gonçalves,<sup>a</sup> B. Mousavi,<sup>b</sup> M. I. M. Prata,<sup>c</sup> S. P. J.  
5 Rodrigues,<sup>d</sup> Daniel Calle,<sup>e</sup> Pilar López-Larrubia,<sup>e</sup> Sebastian Cerdan,<sup>e</sup> Tiago B.  
6 Rodrigues,<sup>f,g</sup> Paula M. Ferreira,<sup>a</sup> L. Helm,<sup>b\*</sup> José A. Martins<sup>a\*</sup> and Carlos F. G. C.  
7 Geraldes<sup>h</sup>

8  
9 <sup>a</sup>Centro de Química, Campus de Gualtar, Universidade do Minho, 4710-057 Braga,  
10 Portugal. E-mail: jmartins@quimica.uminho.pt

11 <sup>b</sup>Laboratoire de Chimie Inorganique et Bioinorganique, Ecole Polytechnique Fédérale  
12 de Lausanne, EPFL-BCH CH-1015 Lausanne, Switzerland. E-mail:  
13 lothar.helm@epfl.ch; Fax: +41 (0)21 693 98 95; Tel: +41 (0)21 693 98 76

14 <sup>c</sup>IBILI and ICNAS, Universidade de Coimbra, Coimbra, Portugal.

15 <sup>d</sup>Chemistry Center and Department of Chemistry, University of Coimbra, 3004-535,  
16 Coimbra, Portugal.

17 <sup>e</sup>Instituto de Investigaciones Biomédicas “Alberto Sols”, CSIC-UAM, Madrid, Spain

18 <sup>f</sup>Cancer Research UK Cambridge Research Institute, Li KaShing Centre, Cambridge  
19 CB2 0RE, United Kingdom.

20 <sup>g</sup>Department of Biochemistry, University of Cambridge, Cambridge CB2 1GA, United  
21 Kingdom.

22 <sup>h</sup>Chemistry Center and Department of Life Sciences, Faculty of Science and  
23 Technology, University of Coimbra, Calçada Martim de Freitas, 3000-393 Coimbra,  
24 Portugal.

25  
26 Corresponding authors:

27 José A. Martins, Centro de Química, Campus de Gualtar, Universidade do Minho,  
28 4710-057 Braga, Portugal.

29 Lothar Helm, École Polytechnique Fédérale de Lausanne, EPFL-BCH CH-1015  
30 Lausanne, Switzerland.

31

32

- 1 Keywords: Gold nanoparticles; Gd<sup>3+</sup> chelates; Contrast Agents; MRI; linkers; ω-thiol
- 2 functionalized DO3A-*N*-(α-amido)propionate chelators; fast water exchange; stability;
- 3 biodistribution; *in vivo* MRI.
- 4

## 1 Abstract

2 The relaxivity displayed by  $Gd^{3+}$  chelates immobilized onto gold nanoparticles is  
3 the result of complex interplay between nanoparticle size, water exchange rate and  
4 chelate structure. In this work we study the effect of the length of  $\omega$ -thioalkyl linkers,  
5 anchoring fast water exchanging  $Gd^{3+}$  chelates onto gold nanoparticles, on the relaxivity  
6 of the immobilized chelates. Gold nanoparticles functionalized with  $Gd^{3+}$  chelates of  
7 mercaptoundecanoyl and lipoyl amide conjugates of the DO3A-*N*-( $\alpha$ -amino)propionate  
8 chelator were prepared and studied as potential CA for MRI. High relaxivities per  
9 chelate, of the order of magnitude  $28\text{-}38\text{ mM}^{-1}\text{s}^{-1}$  (30 MHz, 25 °C) were attained thanks  
10 to simultaneous optimization of the rotational correlation time and of the water  
11 exchange rate. Fast local rotational motions of the immobilized chelates around  
12 connecting linkers (internal flexibility) still limit the attainable relaxivity. The degree of  
13 internal flexibility of the immobilized chelates seems not to be correlated with the  
14 length of the connecting linkers. Biodistribution and MRI studies in mice suggest that  
15 the *in vivo* behavior of the gold nanoparticles is determined mainly by size. Small  
16 nanoparticles (HD= 3.9 nm) undergo fast renal clearance and avoidance of the RES  
17 organs while larger nanoparticles (HD= 4.8 nm) undergo predominantly hepatobiliary  
18 excretion. High relaxivities, allied to chelate and nanoparticle stability and fast renal  
19 clearance *in vivo* suggests that functionalized gold nanoparticles hold great potential for  
20 further investigation as MRI Contrast Agents. This study contributes to understand the  
21 effect of linker length on the relaxivity of gold nanoparticles functionalized with  $Gd^{3+}$   
22 complexes. It is a relevant contribution towards “design rules” for nanostructures  
23 functionalized with  $Gd^{3+}$  chelates as Contrast Agents for MRI and multimodal imaging.

24

25

26

27

28

29

30

31

32

## 1 Introduction

2 MRI is becoming the “central imaging modality” in clinical diagnostic.<sup>1</sup> MRI is based  
3 on the nuclear magnetic resonance phenomenon (NMR). In MRI scans, essentially, the  
4 relaxation times ( $T_1$  and  $T_2$ ) of the water protons of tissues (intrinsically different) are  
5 acquired and reconstructed into tridimensional anatomical images.<sup>2,3</sup> MRI is inherently  
6 non-invasive, makes use of (benign) non-ionizing radiation (static and radiofrequency  
7 magnetic fields), is depth independent and displays superb spatial resolution. Low  
8 detection sensitivity (inherent to the NMR phenomenon) is the main limitation of MRI.<sup>4</sup>  
9 Contrast Agents (CA) are paramagnetic species ( $Gd^{3+}$ ,  $Mn^{2+}$ ,  $Fe^{3+}$ , stable organic  
10 radicals, iron oxide nanoparticles, etc.) that by promoting selective reduction of  $T_1$  or  $T_2$   
11 of the water protons of tissues can generate dramatic contrast enhancements.<sup>5,6</sup> The  
12 selective enhancement of the relaxation rates,  $R_{1,2}$ , ( $R_{1,2} = 1/T_{1,2}$ ), normalized to 1 mM  
13 concentration of paramagnetic centres - relaxivity ( $r_{1,2}$ , units  $mM^{-1} s^{-1}$ ), measures CA  
14 efficacy.<sup>4,7</sup> Approved CA for clinical MRI are either  $Gd^{3+}$  complexes with linear  
15 (DTPA-type) and macrocyclic (DOTA-type) poly(aminocarboxylate) ligands ( $T_1$ -  
16 weighed MRI)<sup>8</sup> or iron oxide nanoparticles (IONPS) stabilized with dextran ( $T_2$ - $T_2^*$ -  
17 weighed MRI).<sup>9</sup> Low molecular weight  $Gd^{3+}$ -based CA display relaxivities of the order  
18 of magnitude  $3\text{-}5\text{ mM}^{-1}\text{ s}^{-1}$  at magnetic fields relevant (currently) for clinical MRI (20-  
19 120 MHz). The Solomon-Bloembergen-Morgan (SBM) theory predicts that very high  
20 relaxivities, of the order of magnitude  $100\text{ mM}^{-1}\text{ s}^{-1}$  at magnetic fields relevant for  
21 clinical imaging (20-120 MHz), are attainable by  $Gd^{3+}$  chelates displaying simultaneous  
22 optimization of the main parameters that govern relaxivity: rotational correlation times  
23 ( $\tau_R$ ), water exchange rate constant ( $k_{ex}$ ) and electron relaxation parameters ( $\tau_v$  and  $\Delta^2$ ).<sup>4,7</sup>  
24 Despite great advancements in the design and synthesis of CA during the past two  
25 decades, the ideal CA- displaying very high relaxivity and safety *in vivo*, targeting  
26 capability and responsiveness coupled to therapeutic properties, is still elusive.<sup>10</sup>

27 The “nanotechnology revolution” is underway with a dramatic impact in many  
28 fields, particularly in medical imaging.<sup>11</sup> Gold nanostructures (nanoparticles,  
29 nanoclusters, nanorods, etc) are finding many applications in chemistry, medicine,  
30 biotechnology and other fields, owing to intrinsic reporting properties (localized  
31 surface plasmon resonance, fluorescence, X-Ray attenuation)<sup>12</sup> coupled to therapeutic  
32 properties (hyperthermia, X-ray sensitization),<sup>13</sup> biocompatibility and safety *in vivo*<sup>14</sup>  
33 and *facile* preparation with tunable size and surface properties by bottom-up

1 methodologies.<sup>15</sup> The first generation of gold nanoparticles (AuNPs) CA made use of,  
2 easy to synthesize, thiol-functionalised Gd(DTPA-*bis*-amide)<sup>16-18</sup> and Gd(DO3A)-type  
3 chelates.<sup>19</sup> Superb relaxivities (per nanoparticle) were attained thanks to chelate  
4 clustering.<sup>16</sup> *In vivo* MRI studies established the merits of AuNPs as CA for MRI,  
5 bimodal MRI/X-ray imaging and as theragnostics (MRI/X-ray sensitization).<sup>16-18,20</sup>  
6 Slow water exchange and fast local rotational motions of the immobilized chelates  
7 around linkers/spacers (chelate flexibility) result in relaxivity enhancements (per  
8 chelate) lower than those expected for Gd<sup>3+</sup> chelates appended to rigid nanosized  
9 objects.<sup>16-18,21,22</sup> Helm and co-workers reported very high relaxivity per chelate  
10 immobilized onto AuNPs (60 mM<sup>-1</sup> s<sup>-1</sup>; 30 MHz, 25 °C), attributed to two exchanging  
11 inner sphere water molecules in Gd(DTTA)-type chelates and complete rigidity of the  
12 chelates immobilized *via* a short aromatic linker.<sup>23</sup> The relaxivity was however, still  
13 limited by slow water exchange. We have demonstrated in previous studies that the  
14 Gd[DO3A-*N*-( $\alpha$ -amino)propionate] chelate and Gd<sup>3+</sup> complexes of amide conjugates of  
15 the DO3A-*N*-( $\alpha$ -amino)propionate chelator display water exchange rates within the  
16 range considered ideal for attaining high relaxivities at intermediate fields, thanks to  
17 “steric compression around the water binding site”.<sup>24,25,26</sup> AuNPs functionalized with the  
18 fast water exchanging chelate Gd[DO3A-*N*-( $\alpha$ -cystamido)propionate] display high  
19 relaxivities at intermediate and high fields (27 and 8.0 mM<sup>-1</sup> s<sup>-1</sup>; 20 and 200 MHz,  
20 respectively, 25 °C) as the result of simultaneous optimization of the rotational  
21 dynamics and water exchange rate.<sup>27</sup> Fast local rotational motions around the cysteine  
22 linker still limit the attainable relaxivity, as demonstrated before for other  
23 macromolecular/nanosized objects such as micelles, dendrimers, polymers, etc.<sup>26,27,28</sup> In  
24 this work we address the effect of the length of the  $\omega$ -thioalkyl linker, anchoring fast  
25 water exchanging Gd[DO3A-*N*-( $\alpha$ -amido)propionate] chelates to gold nanoparticles, on  
26 the relaxivity. Biodistribution and *in vivo* MRI studies with the functionalized AuNPs as  
27 CA are reported also.

28

29

30

31

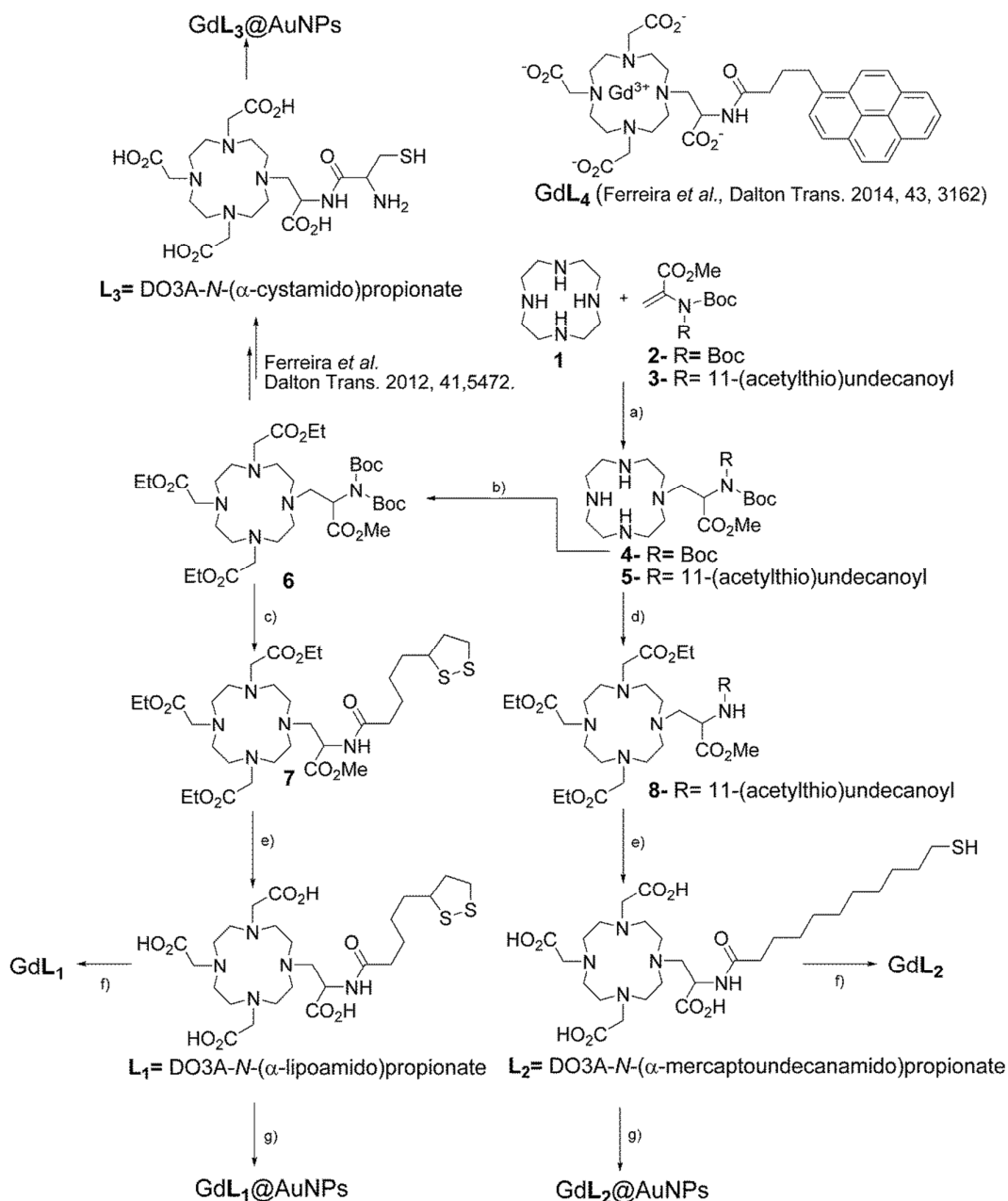
32

33

1 **Synthesis and characterization**

2

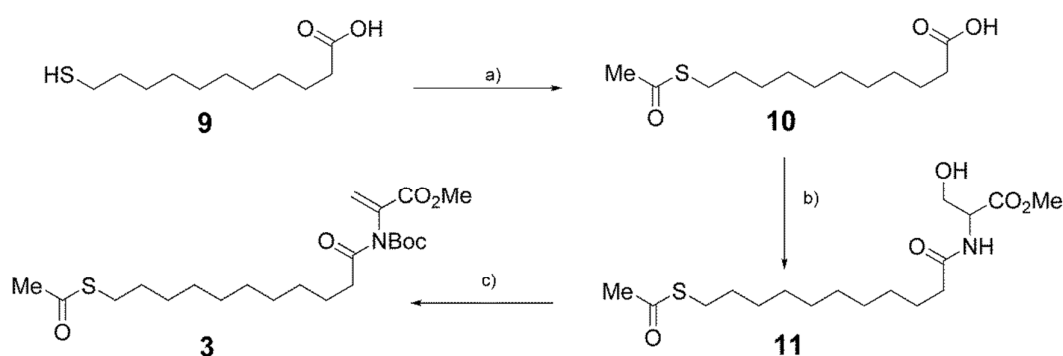
3 Mercaptoundecanoyl and lipoyl conjugates of the DO3A-*N*-( $\alpha$ -amino)propionate  
 4 chelator were synthesized to study the effect of the length of the  $\omega$ -thioalkyl linker on  
 5 the relaxivity of AuNPs functionalized with Gd<sup>3+</sup> chelates (Scheme1).



6

7 **Scheme 1.** Synthetic pathway for  $\omega$ -thioalkyl conjugates of the DO3A-*N*-( $\alpha$ -amino)propionate chelator:  
 8 a) K<sub>2</sub>CO<sub>3</sub>/MeCN; b) ethyl bromoacetate, K<sub>2</sub>CO<sub>3</sub>/MeCN; c) i. TFA/CH<sub>2</sub>Cl<sub>2</sub>, ii. DIPEA/CH<sub>2</sub>Cl<sub>2</sub>, lipoic  
 9 acid, DCC/HOBt; d) i) TFA/DCM, ii. Ethyl bromoacetate, K<sub>2</sub>CO<sub>3</sub>/MeCN; e) i. NaOH aq., ii. Flash  
 10 chromatography silica gel, iii. SEM (Sephadex G10); f) GdCl<sub>3</sub>·6H<sub>2</sub>O; g) i. HAuCl<sub>4</sub>, NaBH<sub>4</sub>, ii.  
 11 GdCl<sub>3</sub>·6H<sub>2</sub>O, iii. SEM (Sephadex G10) followed by dialysis (cellulose tubing MWCO 10 KDa).

1 The lipoic acid conjugate (**L**<sub>1</sub>) was prepared following the synthetic  
 2 methodology reported before for the cysteine conjugate of the DO3A-*N*-( $\alpha$ -  
 3 amino)propionate chelator (**L**<sub>3</sub>).<sup>27</sup> The synthetic pathway excludes, all along, acidic  
 4 conditions likely to promote oligomerization of the chelator through the lipoic acid  
 5 moiety.<sup>29</sup> Deprotection of the fully alkylated orthogonally protected intermediate **6**  
 6 allows direct conjugation of lipoic acid to the preformed DO3A-*N*-( $\alpha$ -amino)propionate  
 7 scaffold.<sup>27</sup> For preparing the 11-mercaptoundecanoyl conjugate (**L**<sub>2</sub>) the preformed  
 8 amide was introduced into the *cyclen* scaffold *via* Michael addition of the *N*-Boc,*N*-(11-  
 9 (acetylthio)undecanoyl)dehydroalanine methyl ester electrophile (**3**).<sup>25,26</sup> Reactive block  
 10 **3** was prepared over 3 steps in 48 % overall yield (Scheme 2).<sup>30</sup>



11

12 **Scheme 2.** Synthetic route for Michael electrophile *N*-Boc,*N*-(11-(acetylthio)undecanoyl)dehydroalanine  
 13 methyl ester (**3**): a) acetic anhydride/pyridine; b) serine methyl ester hydrochloride, HOBT/DCC/NEt<sub>3</sub>; c)  
 14 Boc<sub>2</sub>O/DMAP, dry acetonitrile.

15

16 The thioacetyl protecting group proved easy to install and stable under mild  
 17 alkaline and strong acidic conditions *en route* to **L**<sub>2</sub>. Final deprotection was performed  
 18 in one step by saponification with ethanolic NaOH. Following pH adjustment to  
 19 neutrality with diluted hydrochloric acid, chelators **L**<sub>1</sub> and **L**<sub>2</sub> were adsorbed onto silica  
 20 and purified by flash chromatography followed by Size Exclusion Chromatography  
 21 (SEC) on Sephadex G10 with water elution.

22

23

24

25

26

27

28

29

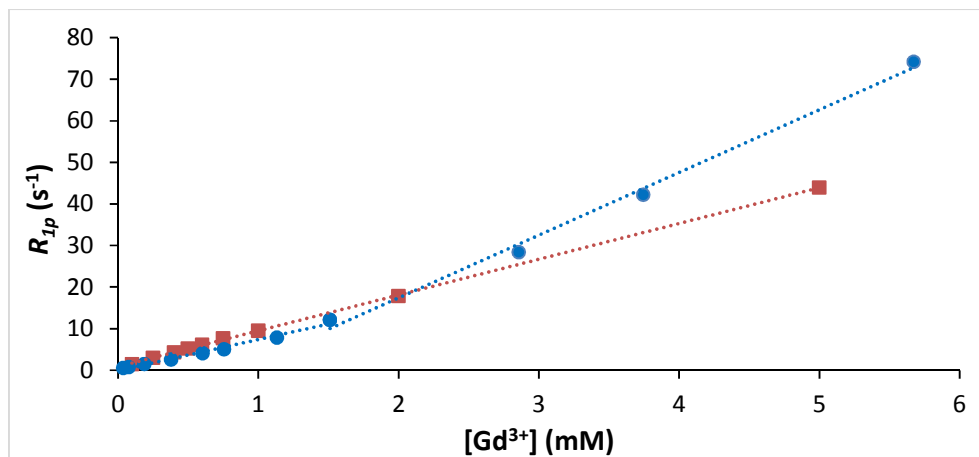


1

2 **Relaxometric studies of GdL<sub>1</sub> and GdL<sub>2</sub>**

3

4 The concentration dependence of the paramagnetic longitudinal water proton relaxation  
 5 rate ( $R_{1p}$ ) was measured for GdL<sub>1</sub> and GdL<sub>2</sub> (20 MHz, 25 °C, pH 7.1) (Figure 1).



6

7

8 **Figure 1.** Concentration dependence of the paramagnetic water proton relaxation rate  $R_{1p} = (R_{1obs} - R_{1d})$  for  
 9 GdL<sub>1</sub> (■) and GdL<sub>2</sub> (●) (20 MHz, 25 °C, pH 7.1).  
 10

11 The relaxation rate data for GdL<sub>1</sub> can be well fitted to a straight line (Equation 1)  
 12 affording a relaxivity of  $8.6 \pm 0.9 \text{ mM}^{-1} \text{ s}^{-1}$  (20 MHz, 25 °C, pH 7.1), characteristic of  
 13 low/intermediate molecular weight chelates in fast rotation in solution. Fitting the  
 14 relaxation rate data of GdL<sub>2</sub> requires two straight lines with different slopes (Equation 1  
 15 and 2). The concentration at the interception of the two lines defines the critical micelle  
 16 concentration- *cmc* ( $cmc = 1.5 \pm 0.3 \text{ mM}$ ).<sup>31</sup>

17

$$18 \quad R_{1p} = R_1^{obs} - R_1^d = r_1^{na} \times c_{Gd} \quad \text{Eq. 1}$$

$$19 \quad R_{1p} = R_1^{obs} - R_1^d = (r_1^{na} - r_1^a)cmc + r_1^a \times c_{Gd} \quad \text{Eq. 2}$$

20

21  $R_1^{obs}$  is the longitudinal relaxation rate measured for the solution,  $R_1^d$  is the  
 22 diamagnetic contribution to the longitudinal relaxation rate (the relaxation rate of pure  
 23 water) and  $C_{Gd}$  is the analytical  $\text{Gd}^{3+}$  concentration.

24 Below the *cmc* GdL<sub>2</sub> is present in solution as monomers (non-aggregated),  
 25 displaying a relaxivity ( $r_1^{na} = 6.6 \pm 0.1 \text{ mM}^{-1} \text{ s}^{-1}$ ; 20 MHz, 25 °C, pH 7.1) characteristic  
 26 of low molecular weight chelates (Equation 1).

1 For GdL<sub>2</sub> at concentrations above the *cmc* the relaxation rate has a contribution  
2 from monomers (at a concentration equal to the *cmc* value) and from the (aggregated)  
3 micellar form ( $r_1^a = 15.1 \pm 0.8 \text{ mM}^{-1} \text{ s}^{-1}$ ; 20 MHz, 25 °C, pH 7.1) (Eq. 2). Self-association  
4 of GdL<sub>2</sub> into micelle-type structures leads to an increase of the effective molecular  
5 volume of the chelate. Slow tumbling in solution (longer rotational correlation times)  
6 translates into substantially higher relaxivity for the aggregated form of GdL<sub>2</sub>  
7 comparing to its monomeric (non-aggregated) form. The relaxivity enhancement for  
8 GdL<sub>2</sub> upon self-assembly is of the same order of magnitude as that reported for the  
9 DOTA-type Gd(DOTASA-C12) chelate functionalized with a C<sub>12</sub> alkyl chain ( $r_1^a = 18.0$   
10  $\text{mM}^{-1} \text{ s}^{-1}$ , 20 MHz, 25 °C)<sup>32</sup>, but significantly lower than that attained by the aggregated  
11 form of the fast water exchanging Gd[DO3A-*N*-( $\alpha$ -pyrenebutanamido)propionate]  
12 chelate (GdL<sub>4</sub> in Scheme 1) ( $r_1^a = 32 \text{ mM}^{-1} \text{ s}^{-1}$ ; 20 MHz; 25 °C).<sup>26</sup> The temperature  
13 dependence of the water proton longitudinal relaxation rate for GdL<sub>1</sub> and GdL<sub>2</sub> (20  
14 MHz, 25 °C) (Figure SI1) indicates that the relaxivity is not limited by slow water  
15 exchange, as demonstrated before for other Gd<sup>3+</sup> chelates of amide conjugates of the  
16 DO3A-*N*-( $\alpha$ -amino)propionate chelator.<sup>24,27</sup> As both GdL<sub>2</sub> and Gd[DO3A-*N*-( $\alpha$ -  
17 pyrenebutanamido)propionate] chelates display fast water exchange, the lower  
18 relaxivity attained by GdL<sub>2</sub> has to be ascribed to higher internal flexibility and/or  
19 smaller size of the GdL<sub>2</sub> micelles (Figure SI2). The pH dependence of the proton  
20 relaxation rate (Figure SI3) and the transmetallation study (Figure SI4) show that GdL<sub>1</sub>  
21 and GdL<sub>2</sub> are stable in the physiological pH range and kinetically inert towards  
22 transmetallation against Zn<sup>2+</sup>.<sup>33</sup>

23

#### 24 **Preparation of gold nanoparticles functionalized with GdL<sub>1</sub> and GdL<sub>2</sub> chelates**

25

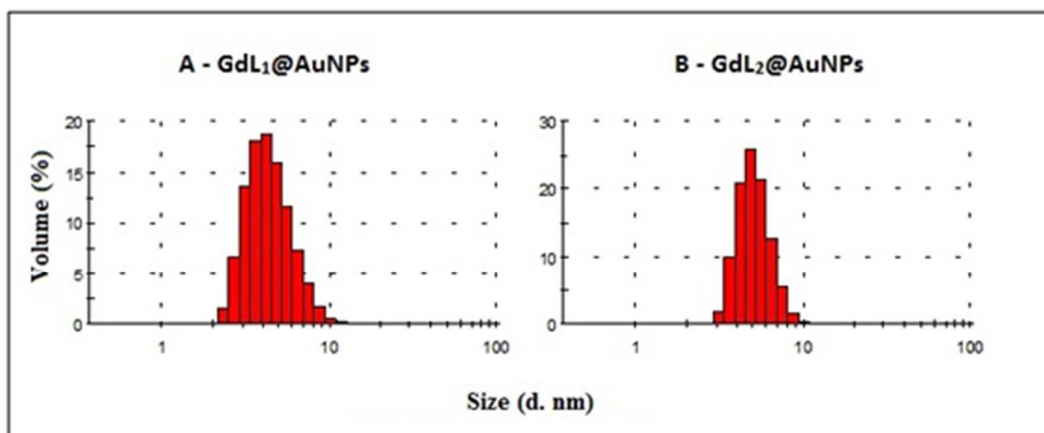
26 A modified Brust's methodology in aqueous solution was employed for preparing  
27 AuNPs functionalized with GdL<sub>1</sub> and GdL<sub>2</sub> chelates.<sup>27,34</sup> Using directly the GdL<sub>1</sub> and  
28 GdL<sub>2</sub> chelates as nanoparticle stabilizers resulted in extensive precipitation upon  
29 addition of the reducing agent (NaBH<sub>4</sub>). Attempts to functionalize citrate-stabilized  
30 AuNPs with GdL<sub>1</sub> and GdL<sub>2</sub> chelates *via* place exchange revealed also unsuccessful.<sup>18</sup>  
31 A two-step methodology, using the L<sub>1</sub> and L<sub>2</sub> chelators as NPs stabilizers, followed by  
32 Gd<sup>3+</sup> complexation, revealed successful for preparing AuNPs functionalized with GdL<sub>1</sub>  
33 and GdL<sub>2</sub> chelates (Scheme 1).<sup>27</sup>

1 Solutions containing equimolar amounts of  $L_1$  or  $L_2$  and  $\text{HAuCl}_4$  turned  
2 immediately dark brown upon addition, in one aliquot, of one molar equivalent of  
3  $\text{NaBH}_4$ . Adding a molar equivalent of  $\text{Gd}^{3+}$ , in relation to the total amount of  $L_1$  or  $L_2$  in  
4 the crude mixture, resulted in stable NPs. Size Exclusion Chromatography (SEC)  
5 (Sephadex G10, elution with water) followed by extensive dialysis against water  
6 (cellulose tubing MWCO 10 000), afforded stable AuNPs functionalized with  $\text{GdL}_1$  and  
7  $\text{GdL}_2$  chelates. A single fraction, including the broad colored band eluting on SEC, was  
8 collected. The absence of (free) uncomplexed  $\text{Gd}^{3+}$  was confirmed by the xylenol  
9 orange test.<sup>35</sup>

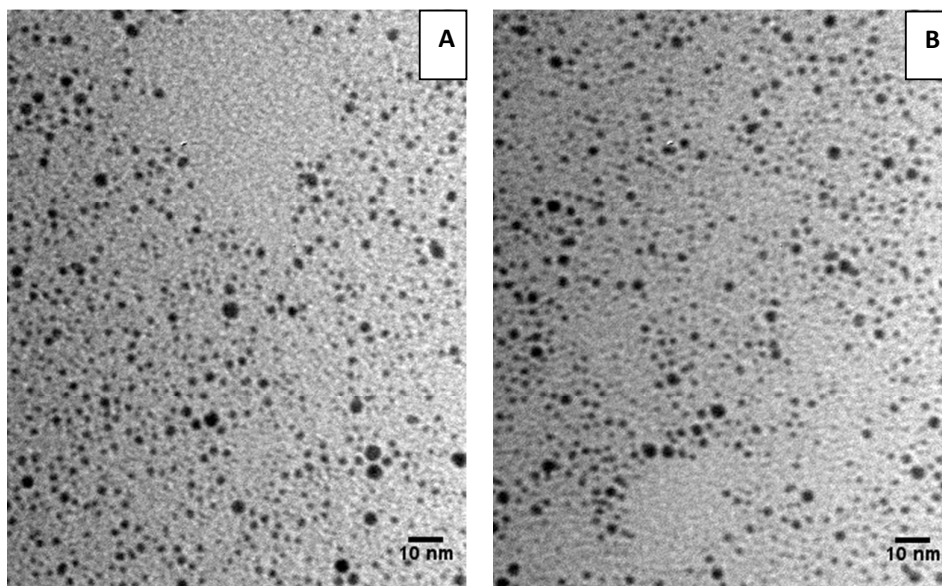
### 11 Characterization of $\text{GdL}_1@AuNPs$ and $\text{GdL}_2@AuNPs$ preparations

12  
13 The Gd content of the functionalized AuNPs was estimated by bulk magnetic  
14 susceptibility measurements<sup>36</sup> and further confirmed by ICP-OES following sample  
15 digestion with *aqua regia* ( $\text{HCl}/\text{HNO}_3$ ; 3/1 v/v) (Table 1).<sup>27,37</sup>

16 The AuNPs were characterized regarding size distribution by Dynamic Light Scattering  
17 (DLS) (Figure 2) and Transmission Electron Microscopy (TEM) (Figure 3).



19  
20  
21 **Figure 2.** Size distribution (% volume) for  $\text{GdL}_1@AuNPs$  (A) and  $\text{GdL}_2@AuNPs$  (B).  
22



1 **Figure 3.** Transmission Electron Microscopy (TEM) for GdL<sub>1</sub>@AuNPs (A) and GdL<sub>2</sub>@AuNPs (B).

2

3 DLS measurements give the hydrodynamic diameter (HD) of NPs, including the  
4 Au nanocrystal core, the chelate monolayer and the immobile ionic layer surrounding  
5 the NPs. An average HD of 4.8 nm (NPs distribution in the range 3-10 nm with a  
6 maximum at 3-4 nm) and 5.9 nm (NPs distribution in the range 2-11 nm with a  
7 maximum at 4-5 nm), was measured for GdL<sub>1</sub>@AuNPs and GdL<sub>2</sub>@AuNPs,  
8 respectively. TEM measurements reveal only the nanocrystal core. The TEM images  
9 obtained for GdL<sub>1</sub>@AuNPs and GdL<sub>2</sub>@AuNPs do not allow to determine the average  
10 diameter of the Au core owing to the very small size of the NPs. From the TEM images  
11 one can only conclude that most GdL<sub>1</sub>@AuNPs and GdL<sub>2</sub>@AuNPs have a nanocrystal  
12 core with a diameter under 2 nm. The average diameter of the Au core of  
13 GdL<sub>1</sub>@AuNPs and GdL<sub>2</sub>@AuNPs (~ 1.0 and 0.9 nm, respectively) was estimated from  
14 the DLS measurements taking into account the thickness of the chelate monolayer,  
15 calculated by PM6 semi-empirical calculations for the most likely conformations of  
16 GdL<sub>1</sub> and GdL<sub>2</sub> bonded to one or two Au atoms (1.9 and 2.5 nm, respectively) (Figure  
17 SI5, Table SI2).<sup>23,24</sup> The absence of a well-defined plasmon absorption band in the UV-  
18 Vis spectra of GdL<sub>1</sub>@AuNPs and GdL<sub>2</sub>@AuNPs (Figure SI6 and SI7), corroborates the  
19 very small size of the NPs core.<sup>38</sup>

20

21

22

1 **Table 1.** Characterization of GdL<sub>1</sub>@AuNPs and GdL<sub>2</sub>@AuNPs

	GdL <sub>1</sub> @AuNPs <sup>a</sup>	GdL <sub>2</sub> @AuNPs <sup>a</sup>	GdL <sub>3</sub> @AuNPs <sup>b</sup>
[Gd] (mM) <sup>c</sup>	0.57	1.30	1.24
HD (nm) <sup>d</sup>	4.8	5.9	3.9
Zeta potential (mV)	-6.3	-13,7	-12.3
D <sub>Au</sub> <sup>e</sup>	1.0	0.9	0.7 <sup>f</sup>

<sup>a</sup>This work; <sup>b</sup>Ref <sup>27</sup>; <sup>c</sup>Determined by ICP-OES; <sup>d</sup>DLS measurements; <sup>e</sup>Estimated from the HD and semi-empirical calculations of the chelate monolayer thickness- see Table SI2; <sup>f</sup>Revised value according to semi-empirical calculations for the length of GdL<sub>3</sub>.

2

3 As L<sub>1</sub>, L<sub>2</sub> and L<sub>3</sub> share the same coordination cage, the length of the linker  
 4 defines the overall wedge-like geometry of the chelator. Shorter linkers originate bulkier  
 5 thiol ligands. Ligand bulkiness increases in the series L<sub>3</sub>>L<sub>1</sub>>L<sub>2</sub> (Figure SI5). Bulkier  
 6 thiols are likely to terminate the growth of AuNPs earlier than less bulky ligands,  
 7 resulting in AuNPs displaying smaller Au cores associated to higher surface curvature.<sup>39</sup>  
 8 This correlation (D<sub>Au</sub> = 1.0, 0.9 and 0.7 nm, for GdL<sub>1</sub>, GdL<sub>2</sub> and GdL<sub>3</sub>@AuNPs) is  
 9 followed roughly by L<sub>2</sub> and L<sub>3</sub>. The discrepancy observed for L<sub>1</sub> can be due to the  
 10 different sulfur binding mode.

11 GdL<sub>1</sub>@AuNPs and GdL<sub>2</sub>@AuNPs were found to be stable in solution for  
 12 extended periods. The NPs could be freeze-dried and re-dissolved without  
 13 aggregation/precipitation. This can be ascribed to the overall negative charge (-1) of the  
 14 immobilized Gd<sup>3+</sup> complexes, resulting in NPs displaying negative zeta-potential  
 15 (Figure SI8).

16

### 17 Relaxometric characterization of GdL<sub>1</sub>@AuNPs and GdL<sub>2</sub>@AuNPs

18

19 The concentration dependence of the proton longitudinal relaxation rate (R<sub>1p</sub>)  
 20 was evaluated for GdL<sub>1</sub>@AuNPs and GdL<sub>2</sub>@AuNPs (r<sub>1</sub> = 29 and 38 mM<sup>-1</sup> s<sup>-1</sup>,  
 21 respectively, 20 MHz, 25 °C, pH 7.1) (Figure SI9).

22 For relevant clinical applications chelates immobilized onto NPs must be stable  
 23 regarding demetallation and inert towards transmetallation with physiological metal  
 24 ions, mainly Zn<sup>2+</sup>.<sup>33</sup> In addition to releasing toxic Gd<sup>3+</sup>, demetallation and  
 25 transmetallation processes of immobilized chelates are likely to trigger particle  
 26 aggregation and precipitation *in vivo*. Stability at low pH is particularly important as  
 27 protonation-assisted mechanisms have been implicated in demetallation, presumably

1 followed by transmetallation with serum ions, of macrocyclic Gd(DOTA)-type  
2 chelates.<sup>33,40,41</sup> The pH dependence of the protonic relaxation rate ( $R_{1p}$ ) was evaluated  
3 for GdL<sub>1</sub>@AuNPs and GdL<sub>2</sub>@AuNPs in the pH range 3-10 (Figure SI10).

4 The kinetic stability of the immobilized chelates (and entire nanoparticles) was  
5 evaluated by challenging GdL<sub>1</sub>@AuNPs and GdL<sub>2</sub>@AuNPs with Zn<sup>2+</sup> ions in  
6 phosphate buffer (Figure SI11 and Figure SI12).<sup>33</sup> According to the criteria set by  
7 Muller and co-workers, the immobilized chelates (and whole NPs) can be classified as  
8 kinetically inert and thermodynamically stable.<sup>33</sup> The pH stability and kinetic inertness  
9 indicate that the NPs are potentially safe for *in vivo* applications.

10

### 11 Nuclear Magnetic Relaxation Dispersion Profiles

12

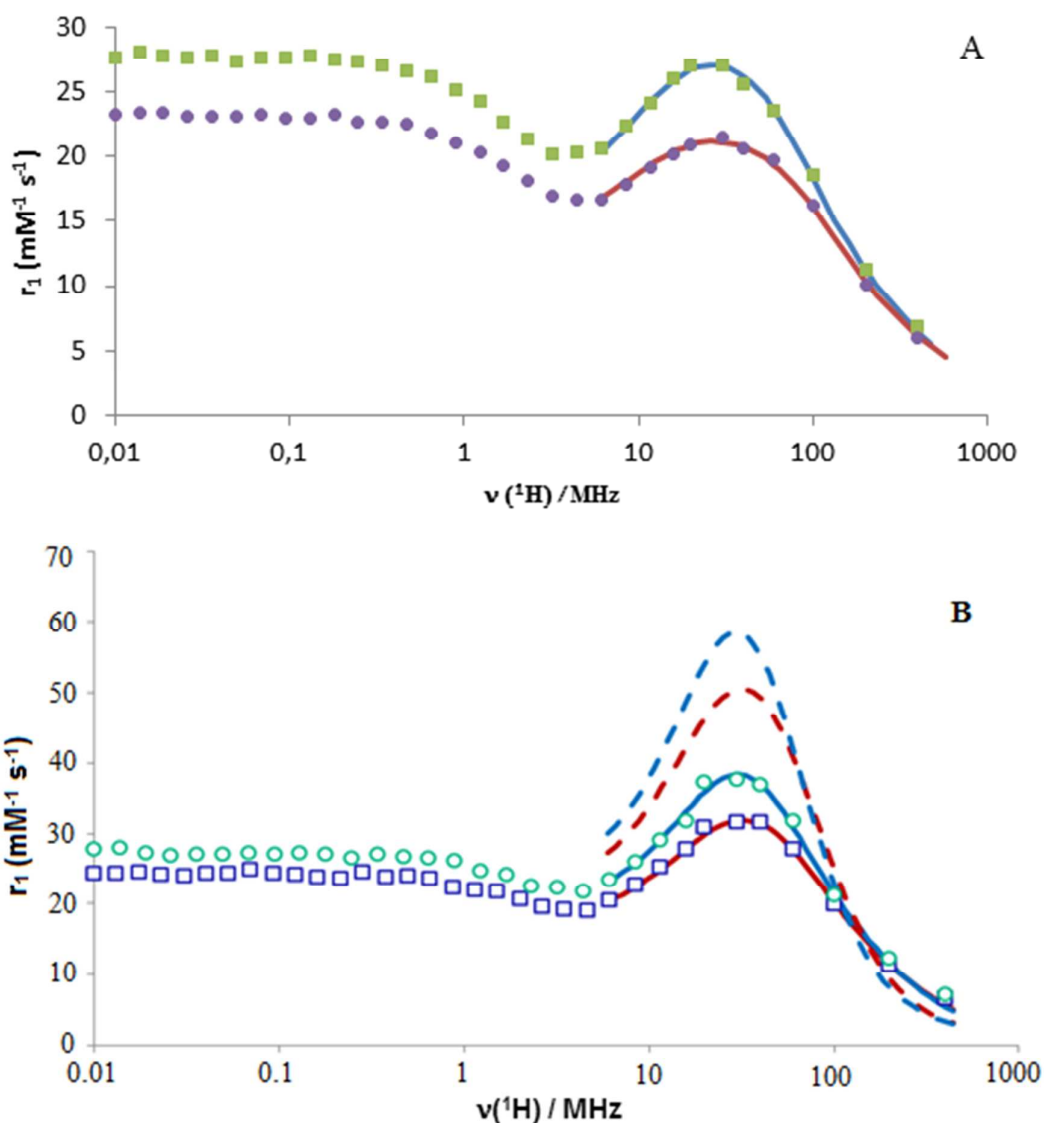
13 The magnetic field dependence of the proton relaxivity ( $r_1$ ) (Nuclear Magnetic  
14 Relaxation Dispersion - NMRD profiles) was obtained for GdL<sub>1</sub>@AuNPs and  
15 GdL<sub>2</sub>@AuNPs in the *Larmor* frequency range 0.01-400 MHz. The most important  
16 parameters that govern relaxivity are the hydration number ( $q$ ), the water exchange rate  
17 constant ( $k_{ex}$ ), the rotational correlation time ( $\tau_R$ ) and the electron relaxation parameters  
18 ( $\tau_v$  and  $\Delta^2$ ).<sup>4,7</sup> The number of water molecules in the first coordination sphere, the water  
19 exchange rate and the rotational correlation time can be tuned by chelate design. Clear  
20 rules to tune the electron relaxation parameters are still elusive.<sup>42</sup> Treating chelates  
21 immobilised onto macromolecular/nanosized objects (micelles, proteins, polymers,  
22 dendrimers, nanoparticles, viral particles) as rigid entities, often fails to deliver reliable  
23 parameters from the fitting of the NMRD profiles to the SBM theory. In fact, it is  
24 necessary to assume in the fittings that the interactions that generate the relaxation are  
25 influenced by both fast local rotational motions ( $\tau_{Rlocal}$ ) of the immobilized chelates  
26 around linkers/spacers and a slower, global motion, common to the entire object  
27 ( $\tau_{Rglobal}$ ). The degree of spatial restriction of the local motion (interpreted as chelate  
28 flexibility), is measured by the generalized, model independent order parameter-  $S^2$ . The  
29 order parameter can assume values in the range 0-1:  $S^2=0$  if the internal motions are  
30 isotropic,  $S^2=1$  if the internal motions are completely restricted.<sup>43</sup>

31

32 In this work, it was assumed in the fittings that the immobilised GdL<sub>1</sub> and GdL<sub>2</sub>  
33 complexes have one inner sphere water molecule ( $q = 1$ ) like other Gd<sup>3+</sup> complexes of  
the DO<sub>3</sub>A-*N*-( $\alpha$ -amino/amido)propionate family.<sup>24-26</sup> The water exchange rate constant

1 and its activation enthalpy ( $k_{\text{ex}}^{298}$ ,  $\Delta H^\ddagger$ ) were fixed to values determined for the  
 2 analogous Gd[(DO3A-*N*-( $\alpha$ -benzoylamido)propionate)] chelate.<sup>25</sup>

3 The fittings (continuous lines in Figure 4) are restricted to frequencies above 6  
 4 MHz as the SBM theory is not suitable for describing the rotational dynamics of slow-  
 5 rotating objects at low magnetic fields. The best fit parameters for GdL<sub>1</sub>@AuNPs and  
 6 GdL<sub>2</sub>@AuNPs, obtained from the analysis of <sup>1</sup>H NMRD data, are represented in Figure  
 7 4 and summarized in Table 2.



8  
 9  
 10 **Figure 4.** <sup>1</sup>H Nuclear Magnetic Relaxation Dispersion (NMRD) profiles for: **A-** GdL<sub>1</sub>@AuNPs (0.56  
 11 mM; pH 7.0) 25 °C (■) and 37 °C (●); **B-** GdL<sub>2</sub>@AuNPs (1.30 mM; pH 7.0); 25 °C (○) and 37 °C (□).  
 12 The fitted curves are represented as continuous lines. The broken lines are the result of simulations using  
 13 the same parameters as in Table 2, but assuming total rigidity ( $S^2=1$ ) of the immobilized chelates.  
 14

1 **Table 2.** Best fit parameters obtained for GdL<sub>1</sub>@AuNPs and GdL<sub>2</sub>@AuNPs from the fitting of the <sup>1</sup>H  
 2 NMRD profiles to the SMB theory, including the Lipari-Szabo approach for internal flexibility.  
 3

	GdL <sub>1</sub> @AuNPs	GdL <sub>2</sub> @AuNPs
Parameters	Value	Value
$q$	<u>1</u>	<u>1</u>
$\Delta H^{\ddagger}$ [J/mol]	<u>17</u>	<u>17</u>
$k_{\text{ex}}^{298}$ [ $10^7 \text{ s}^{-1}$ ]	<u>5.14</u>	<u>5.14</u>
$E_{\text{R}}$ [kJ/mol] (global)	19.4±1.1	18±3.6
$\tau_{\text{RH}}^{298}$ [ps] (global)	1900±140	3500±940
$E_{\text{R}}$ [kJ/mol] (local)	<u>20</u>	<u>18</u>
$\tau_{\text{RH}}^{298}$ [ps] (local)	460±50	970±230
$S^2$	0.41 ± 0.04	0.42±0.12
$E_{\text{V}}$ [kJ/mol]	<u>1</u>	<u>1</u>
$\tau_{\text{V}}^{298}$ [ps]	27±4	17± 3
$E_{\text{H}}^{298}$ [ $10^{-10} \text{ m}^2 \text{ s}^{-1}$ ]	<u>23</u>	<u>23</u>
$E_{\text{DGH}}$ [kJ/mol]	<u>20</u>	<u>20</u>
Gd-O [Å]	<u>2.5</u>	<u>2.5</u>
$\Delta^2$ [ $10^{20} \text{ s}^{-2}$ ]	0.044±0.002	0.065±0.004
Gd-HW 1 <sup>st</sup> [Å]	<u>3.1</u>	<u>3.1</u>
Gd-HW 2 <sup>nd</sup> [Å]	<u>3.6</u>	<u>3.6</u>

4  
 5 **Table 3.** Selected molecular parameters for GdL<sub>1</sub>@AuNPs and GdL<sub>2</sub>@AuNPs and other systems  
 6 reported in the literature and discussed in the manuscript.

Parameter	GdL <sub>1</sub> @AuNPs <sup>a</sup>	GdL <sub>2</sub> @AuNPs <sup>a</sup>	GdL <sub>3</sub> @AuNPs <sup>b</sup>	GdL <sub>4</sub> <sup>c</sup>
$q$	<u>1</u>	<u>1</u>	<u>1</u>	<u>1</u>
$k_{\text{ex}}^{298}$ [ $10^7 \text{ s}^{-1}$ ]	<u>5.14</u>	<u>5.14</u>	5.14	6.2
$\tau_{\text{g}}^{298}$ [ps]	1900	3500	2470	3780
$\tau_{\text{lo}}^{298}$ [ps]	460	970	177	930
$S^2$	0.41	0.42	0.48	0.24
HD (nm) <sup>d</sup>	4.8	5.9	3.9	49 <sup>e</sup>
$r_{\text{I}}$ (mM <sup>-1</sup> s <sup>-1</sup> )	$27^{f,h}$ 11.2 <sup>f,i</sup>	$38^{f,h}$ 8.4 <sup>f,i</sup>	$28^{f,h}$ 8.5 <sup>f,i</sup>	$32^{g,h}$ n.d.

<sup>a</sup> This work; <sup>b</sup> Ref 27; <sup>c</sup> Ref 26; <sup>d</sup> From DLS measurements; <sup>e</sup> Z-average from a bimodal distribution of particles; <sup>f</sup> Relaxivity per chelate; <sup>g</sup> Relaxivity of the aggregated form; <sup>h</sup> 20 MHz, 25 °C; <sup>i</sup> 200 MHz, 37 °C.

7

8

9 The NMRD profiles are characteristic of macromolecular objects in slow  
 10 rotation, confirming the immobilization of the GdL<sub>1</sub> and GdL<sub>2</sub> chelates onto gold



1 nanocrystals: a plateau in the frequency range 0.01 to 1 MHz, a simple dispersion at  
2 about 1-10 MHz and a broad hump centered at 20-60 MHz.

3 The AuNPs prepared in this work display exceptional relaxivities (per Gd<sup>3+</sup>  
4 chelate) ( $r_{1max} = 27$  and  $38 \text{ mM}^{-1} \text{ s}^{-1}$  for GdL<sub>1</sub>@AuNPs and GdL<sub>2</sub>@AuNPs, respectively;  
5 30 MHz, 25 °C), much higher than those reported by other authors for AuNPs  
6 functionalized with monoaquated ( $q = 1$ ) Gd<sup>3+</sup> complexes.<sup>16,19,21</sup> The temperature  
7 dependence of the relaxivity, higher relaxivity at lower temperature, for both  
8 GdL<sub>1</sub>@AuNPs and GdL<sub>2</sub>@AuNPs, indicates that the water exchange rate is not limiting  
9 the relaxivity. The superb relaxivities attained can be ascribed to simultaneous  
10 optimization of the water exchange rate (fast water exchange regime) and of the  
11 rotational correlation time. The value obtained for the order parameter ( $S^2 \sim 0.40$ )  
12 indicates that fast local motions of the chelates anchored onto the Au core are still  
13 limiting the relaxivity. Simulations, using the same parameters as on Table 3, but  
14 assuming total rigidity of the immobilized chelates ( $S^2 = 1$ ), afford much higher  
15 relaxivities (of the order of magnitude  $60 \text{ mM}^{-1} \text{ s}^{-1}$ ; 20 MHz; 25 °C) for GdL<sub>2</sub>@AuNPs.  
16 The higher relaxivity attained by GdL<sub>2</sub>@AuNPs, comparing to GdL<sub>1</sub>@AuNPs and  
17 GdL<sub>3</sub>@AuNPs, has to be ascribed to its significantly larger global rotational correlation  
18 time ( $\tau_{Rg}$ ), reflecting the larger size (hydrodynamic diameter) of the GdL<sub>2</sub>@AuNPs  
19 nanoparticles. In fact, the length of the thioalkyl linker seems not to have much  
20 influence on the internal flexibility of the immobilized chelates: the order parameter  $S^2$   
21 is identical for GdL<sub>1</sub>@AuNPs and GdL<sub>2</sub>@AuNPs, despite the longer linker anchoring  
22 GdL<sub>2</sub> to the Au core. Moreover, the shorter cysteine linker anchoring GdL<sub>3</sub> to the Au  
23 core (possibly in a bidentate (N, S) fashion similar to GdL<sub>1</sub> (S,S)), results only in  
24 slightly higher rigidity of the immobilized chelates. Despite the limiting effect of the  
25 internal rotational motions, chelate immobilization onto AuNPs results in relaxivity  
26 enhancements of more than 300% for GdL<sub>1</sub> and over 500% for GdL<sub>2</sub> (comparing to its  
27 monomeric form), attributed to simultaneous optimization of  $\tau_R$  and  $k_{ex}$ . Moreover,  
28 GdL<sub>2</sub> immobilized onto AuNPs displays substantially higher relaxivity than the  
29 aggregated (micellar) form of GdL<sub>2</sub> ( $38$  vs  $15 \text{ mM}^{-1} \text{ s}^{-1}$ ; 20 MHz, 25 °C). The micellar  
30 form of the Gd[DO3A-*N*-( $\alpha$ -pyrenebutanamido)propionate] chelate (GdL<sub>4</sub>) (sharing the  
31 same coordination cage with GdL<sub>1,2,3</sub>) is significantly more flexible ( $S^2 = 0.24$  vs  $0.42$ )  
32 than the Au-anchored GdL<sub>1</sub> and GdL<sub>2</sub> chelates. Accordingly, GdL<sub>2</sub>@AuNPs, displaying  
33 a  $\tau_{Rg}$  value similar to the aggregated form of GdL<sub>4</sub>, exhibits higher relaxivity ( $38$  vs  $32$

1 mM<sup>-1</sup> s<sup>-1</sup>; 20 MHz, 25 °C, for GdL<sub>2</sub>@AuNPs and for the aggregated form of GdL<sub>4</sub>,  
 2 respectively).<sup>26</sup>

3 Covalent immobilization of Gd<sup>3+</sup> chelates onto AuNPs seems more effective in  
 4 attaining high relaxivities, than chelate self-assembly into micelle-type structures,  
 5 owing to higher restriction of internal rotational motions.

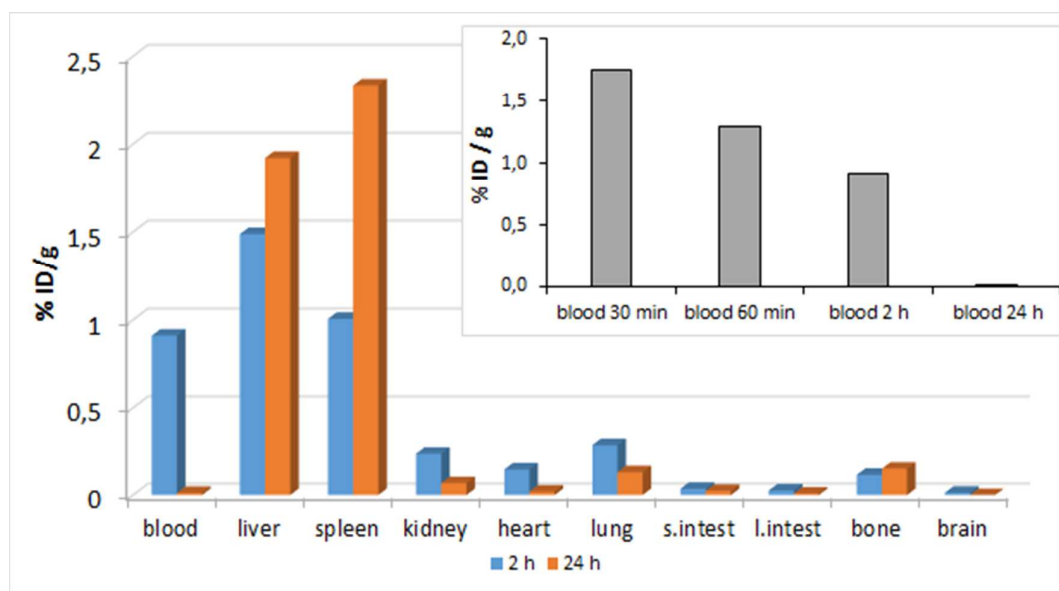
6 The work reported here addresses explicitly the effect of linker length on the  
 7 relaxivity of AuNPs functionalized with Gd<sup>3+</sup> chelates, contributing to the “rational  
 8 design” of nanomaterials as CA for MRI/multimodal imaging.<sup>44</sup>

9

### 10 Biodistribution studies

11 The biodistribution of [<sup>153</sup>Sm]L<sub>1</sub>@AuNPs in Wistar rats was obtained at 2 and 24 hours  
 12 post-injection (Figure 6).

13



14

15 **Figure 6.** Biodistribution of [<sup>153</sup>Sm<sup>3+</sup>]L<sub>1</sub>@AuNPs in Wistar rats, stated as percent of injected dose per  
 16 gram of organ (% ID/ g): a) 2 and b) 24 hour post-injection. Inset - time evolution of the activity in the  
 17 blood. The results are from a group of four animals in each experiment.

19

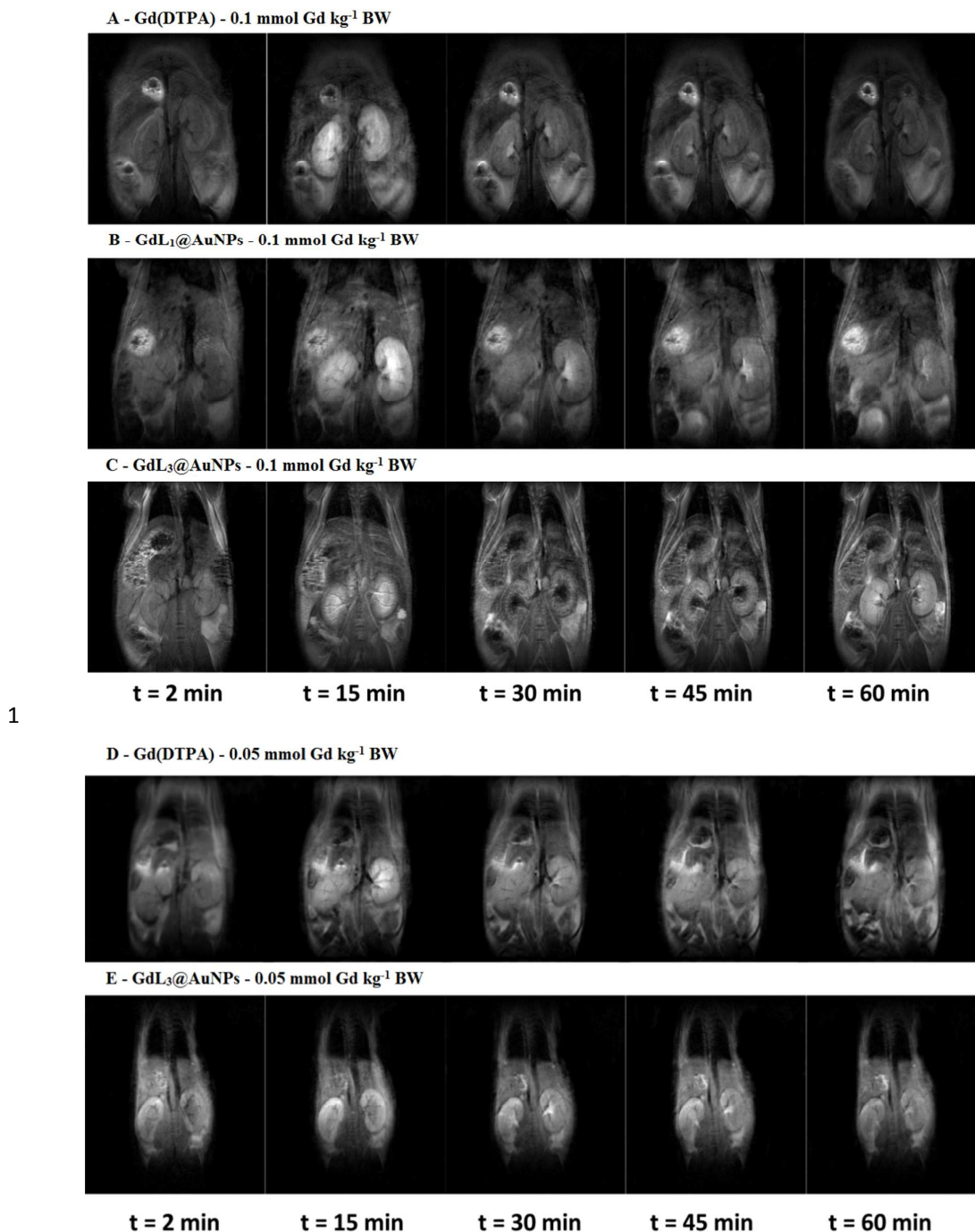
20 The activity in the blood was measured after 30 minutes, 60 minutes, 2 and 24  
 21 hours (inset in Figure 6) revealing fast clearance of activity from the blood with a  
 22 reduction of approximately 50% between 30 minutes and two hours. After 2 hours post-  
 23 injection, the NPs are mainly found in the organs of the reticulo-endothelial system  
 24 (RES), liver and spleen, and to a lesser extent in the blood and lungs. These results  
 suggest that the nanoparticles are cleared mainly by phagocytosis by the macrophage

1 rich organs, liver and spleen, with a less important contribution from renal  
2 elimination.<sup>20,26,45</sup> This is in accordance with what was found by MRI for  
3 GdL<sub>1</sub>@AuNPs (see below).

4 At 24 hours post-injection significant activity is found only in the organs of the  
5 reticulo-endothelial system, RES. The activity approximately doubled in the spleen,  
6 showing only a slight increase in the liver. The activity in the bones at 24 hours post-  
7 injection is very low, suggesting that the rate of chelate demetallation and formation of  
8 insoluble metal colloids *in vivo* is very low.

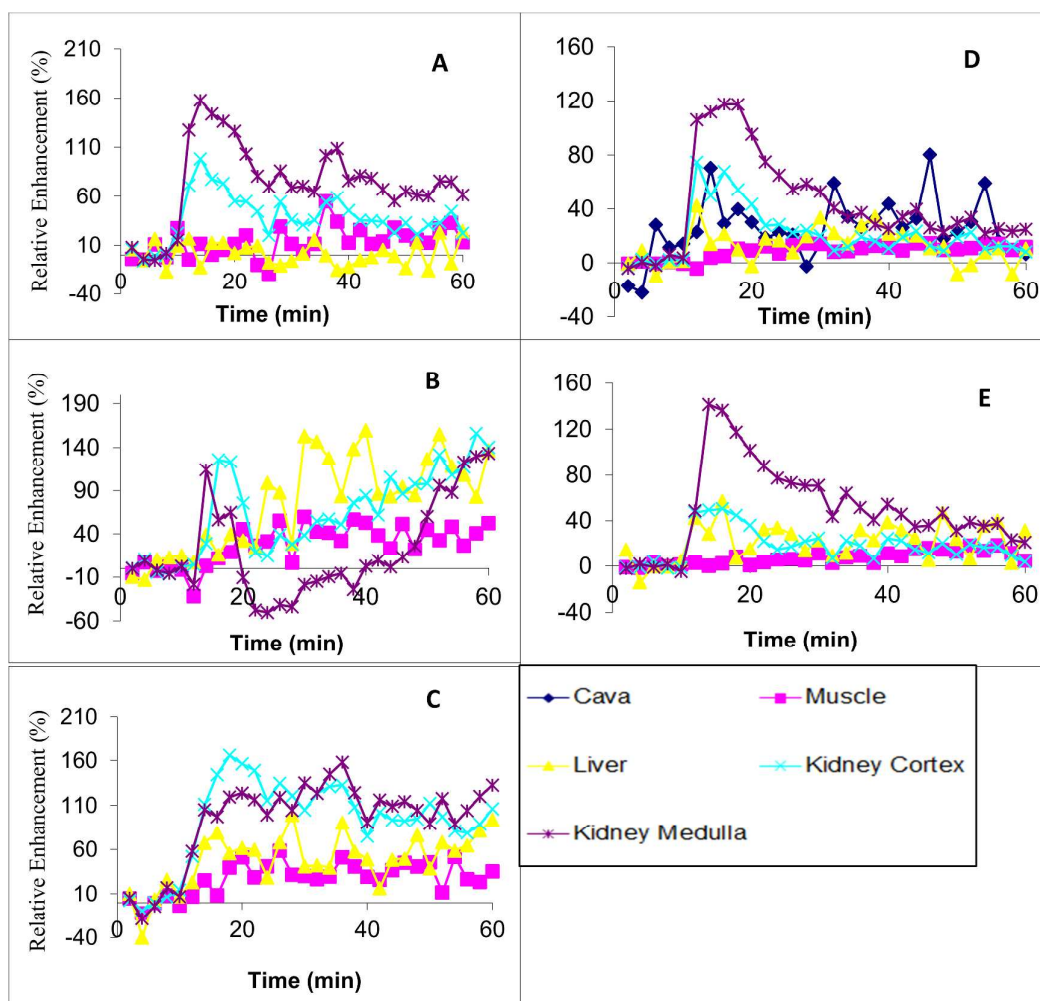
### 9 10 **MRI Studies**

11  
12 MRI studies were performed in male Swiss mice (~ 20 g) in a preclinical  
13 imaging platform (PharmaScan) operating at 7.0 Tesla (300 MHz). A Dynamic Contrast  
14 Enhancement (DCE) study was performed with GdL<sub>1</sub>@AuNPs (0.1 mmol Gd/kg body  
15 weight) and GdL<sub>3</sub>@AuNPs (0.1 and 0.05 mmol Gd/kg body weight) and for  
16 comparison purposes with Gd(DTPA) (Magnetvist<sup>®</sup>, Bayer) at the same doses (Figure  
17 7). Figure 7 shows a representative series of T<sub>1</sub>-weighted spin-echo coronal images. In  
18 the pre-injection images, the kidney structures (cortex, inner and outer medulla) and  
19 adjacent tissues appear dark. After bolus injection in the vascular system, a strong signal  
20 enhancement was observed in the kidneys for Gd(DTPA), GdL<sub>1</sub>@AuNPs and  
21 GdL<sub>3</sub>@AuNPs as result of T<sub>1</sub> shortening. A much slighter signal enhancement was  
22 observed in the liver. Both NPs follow mainly renal elimination by glomerular filtration,  
23 with significant hepatobiliary contribution to excretion seen for GdL<sub>1</sub>@AuNPs only.  
24



3 **Figure 7.** Representative coronal T<sub>1</sub>-weighted spin echo MR images of mice before and after injection of  
 4 contrast agents: (A) Gd(DTPA) (0.1 mmol Gd kg<sup>-1</sup> BW), (B) GdL<sub>1</sub>@AuNPs (0.1 mmol Gd kg<sup>-1</sup> BW), (C)  
 5 GdL<sub>3</sub>@AuNPs (0.1 mmol Gd kg<sup>-1</sup> BW); (D) Gd(DTPA) (0.05 mmol Gd kg<sup>-1</sup> BW), (E) GdL<sub>3</sub>@AuNPs  
 6 (0.05 mmol Gd kg<sup>-1</sup> BW).  
 7

8           The time course of the average intensity (mean values of groups of four animals)  
 9 within different regions of interest (ROIs) placed on the several organs (Figure 8)  
 10 allows to understand better the features of Figure 7.



1  
2  
3 **Figure 8.** Time course of signal intensity, up to 60 min post-injection, for several regions of interest,  
4 relative to the initial value, during dynamic contrast enhancement MRI experiments in rats administrated  
5 with: (A) Gd(DTPA) ( $0.1 \text{ mmol kg}^{-1} \text{ BW}$ ) and (B) GdL<sub>1</sub>@AuNPs ( $0.1 \text{ mmol kg}^{-1} \text{ BW}$ ), (C)  
6 GdL<sub>3</sub>@AuNPs ( $0.1 \text{ mmol kg}^{-1} \text{ BW}$ ); (D) Gd(DTPA) ( $0.05 \text{ mmol kg}^{-1} \text{ BW}$ ); (E) GdL<sub>3</sub>@AuNPs ( $0.05$   
7  $\text{mmol kg}^{-1} \text{ BW}$ ). The time courses are data from mean values of four animals.  
8

9 In order to compare the results for all the animals under study ( $n = 4$ ), the data  
10 were normalized by calculating the mean relative enhancement of each ROI. The  
11 scattering in the time course curves was caused by animal respiratory motion. The  
12 relative enhancement obtained with Gd(DTPA) at  $0.1 \text{ mmol kg}^{-1} \text{ BW}$  dose (Figure 8A),  
13 increased almost immediately after intravenous injection, from 0 up to about 160% in  
14 the kidney medulla and 100% in the kidney cortex, followed by a steady decrease to  
15 values around 60% and 30%, respectively, within 60 minutes. This time course is in  
16 agreement with the literature for the Gd(DTPA) and Gd(DOTA) low molecular weight  
17 CA.<sup>46,47</sup>

1           The enhancement profiles of GdL<sub>1</sub>@AuNPs (Figure 8B) and GdL<sub>3</sub>@AuNPs  
2 (Figure 8C) at 0.1 mol Gd kg<sup>-1</sup> BW dose are considerably different from the  
3 enhancement profile of Gd(DTPA) at the same concentration: there is an immediate  
4 enhancement of the kidney structures (cortex and medulla) followed by a steady liver  
5 enhancement. For GdL<sub>3</sub>@AuNPs at 0.1 mmol Gd kg<sup>-1</sup> BW dose (Figure 8C) is  
6 noticeable a fast and strong enhancement of the kidney medulla and kidney cortex (~  
7 150%) which slowly decreases to ~100% over the time course of the experiment. A  
8 much lower muscle and liver enhancement is also noticeable. Reducing the dose of  
9 GdL<sub>3</sub>@AuNPs to 0.05 mmol Gd Kg<sup>-1</sup> BW results in an imaging profile virtually  
10 equivalent to Gd(DTPA): fast renal elimination with negligible hepatobiliary  
11 contribution (Figure 8D and 8E for Gd(DTPA) and GdL<sub>3</sub>@AuNPs, respectively). There  
12 is a fast enhancement of the kidney cortex (~150 % at 20 minutes) which steadily  
13 decreases over the time course of the experiment. These results strongly suggest that  
14 while GdL<sub>1</sub>@AuNPs is mostly eliminated through hepatobiliary excretion, or is taken  
15 up by resident macrophages (Kupfer cells) in liver, GdL<sub>3</sub>@AuNPs behaves *in vivo* as a  
16 low molecular weight CA following mainly renal elimination. The steady, liver and  
17 presumably spleen enhancement observed with GdL<sub>1</sub>@AuNPs is in sharp contrast to  
18 the “clean” renal elimination observed for GdL<sub>3</sub>@AuNPs. This behaviour can only be  
19 explained by the difference in size between GdL<sub>1</sub>@AuNPs and GdL<sub>3</sub>@AuNPs- average  
20 HD 4.8 and 3.9 nm, respectively, stressing the complex interplay between the physical-  
21 chemical properties of nanostructures and *in vivo* behaviour.

22       The animal MRI studies were performed at high field (300 MHz, 7 Tesla). This study  
23 illustrates the mismatch between the performance of macromolecular/nanosized CA,  
24 optimized for intermediate fields (20-60 MHz), and the trend for increasingly higher  
25 magnetic field imagers. The overwhelming advantage of the AuNPs, over low  
26 molecular weight CA at intermediate fields (20-60 MHz), is partially eroded at higher  
27 magnetic fields (Figure 4).<sup>48</sup> Nonetheless, the AuNPs studied in this work still exhibit  
28 relaxivities significantly higher than Gd(DTPA) at high fields (11.2, 8.4 vs ~ 2 mM<sup>-1</sup> s<sup>-1</sup>  
29 for GdL<sub>1</sub>@AuNPs and GdL<sub>2</sub>@AuNPs, respectively, and Gd(DTPA), 200 MHz, 25 °C ).

30  
31  
32  
33  
34

## 1 **Conclusions**

2 In this work we extend the synthetic methodologies developed before for AuNPs  
3 functionalized with stable fast water exchanging  $Gd^{3+}$  chelates as high relaxivity,  
4 potentially safe CA for *in vivo* MRI. Two novel ligands were designed to investigate the  
5 role of the length of the  $\omega$ -thioalkyl linker, anchoring the coordination cage to the gold  
6 nanocrystal, on the relaxivity. Superb relaxivities at magnetic fields relevant for clinical  
7 imaging (27 and 38  $mM^{-1} s^{-1}$ , 30 MHz, 25 °C, for  $GdL_1@AuNPs$  and  $GdL_2@AuNPs$ ,  
8 respectively) were obtained thanks to simultaneous optimization of the  
9 rotational correlation time and of the water exchange rate. Relaxivities, still relevant for  
10 clinical high field applications (of the order of magnitude 10  $mM^{-1} s^{-1}$ ; 200 MHz, 37 °C)  
11 were attained also. The relaxivity is still limited by internal flexibility of the  
12 immobilized chelates. The degree of internal flexibility of the immobilized chelates  
13 (measured by the order parameter  $S^2$ ) seems not to be determined by the length of the  
14 linker, presumably owing to the high surface curvature of the NPs. A MRI study in mice  
15 demonstrated that while  $GdL_3@AuNPs$  (HD = 3.9 nm) behaves *in vivo* much like the  
16 low molecular weight CA  $Gd(DTPA)$ , undergoing fast renal elimination without liver  
17 (and presumably spleen) uptake,  $GdL_1@AuNPs$  (HD = 4.8 nm) shows considerable  
18 hepatobiliary contribution to elimination. A biodistribution study in rats using the  
19 surrogate  $^{153}SmL_1@AuNPs$  tracer confirmed extensive activity uptake and  
20 accumulation over time in the liver and spleen.

21 The  $GdL_3@AuNPs$  CA, amenable to further elaboration with targeting moieties,  
22 seems particularly promising for *in vivo* MRI applications.

23 The work reported is a relevant contribution towards the design of nanomaterials  
24 functionalized with  $Gd^{3+}$  chelates as very high relaxivity/multimodal CA for MRI.<sup>44</sup>

25

26

27

## 1 **Experimental**

### 2 **Materials and methods**

3

4 Chemicals were purchased from Sigma-Aldrich and used without further purification.  
5 *Cyclen* was purchased from Chematech, France. Analytical grade solvents were used  
6 and not further purified, unless specified. Reactions were monitored by TLC on silica  
7 gel by examination under UV light (250 and 365 nm) and staining with iodine vapour  
8 and Ellman's reagent. Preparative chromatography was carried out on Silica Gel 60  
9 (230-400 mesh). Ion exchange chromatography was performed on Dowex 1X2-100-  
10 OH<sup>-</sup> (50-100 mesh) resin. Size Exclusion Chromatography (SEC) was performed on  
11 Sephadex G10 (40-120  $\mu$ m) with water elution. Dialysis was performed against water  
12 on cellulose membranes (MWCO 10 KDa). UV-VIS spectra were acquired with a  
13 Shimadzu UV-2501PC spectrophotometer. The size distribution and zeta potential of  
14 the AuNPs was determined with a Malvern Zetasizer, NANO ZS (Malvern Instruments  
15 Limited, UK), using a He-Ne laser (wavelength of 633 nm) and a detector angle of 173°.  
16 TEM experiments were performed with a JEOL JEM1200EXII microscope at Bath  
17 University, UK. Mass spectrometry was performed at CACTI - Vigo, Spain.

18 <sup>1</sup>H and <sup>13</sup>C NMR spectra were run on Varian Unity Plus 300, Bruker Avance-3  
19 400 Plus and Varian VNMRS 600 NMR spectrometers. Chemical shifts ( $\delta$ ) are given in  
20 ppm relative to the CDCl<sub>3</sub> solvent (<sup>1</sup>H,  $\delta$  7.27; <sup>13</sup>C 77.36) as internal standard. For <sup>1</sup>H  
21 and <sup>13</sup>C NMR spectra recorded in D<sub>2</sub>O, chemical shifts ( $\delta$ ) are given in ppm, relative to  
22 TSP as internal reference (<sup>1</sup>H,  $\delta$  0.0) and *tert*-butanol as external reference (<sup>13</sup>C, CH<sub>3</sub>  $\delta$   
23 30.29), respectively.

24

### 25 **Preparation of Lipoic acid conjugate DO<sub>3</sub>A-*N*-( $\alpha$ -lipoamido)propionate - L<sub>1</sub>**

26

### 27 **Synthesis of ((5-(1,2-dithiolan-3-yl)-2-pentanamido)methoxycarbonylethyl)-4,7,10-** 28 ***tris*-(ethoxycarbonylmethyl)-1,4,7,10-tetraazacyclododecane - fully protected** 29 **conjugate 7.**

30 Orthogonally protected compound **6** was synthesized as described before by us.<sup>27</sup> A  
31 solution of compound **6** (85 mg; 1.12 mmol) in a mixture DCM/TFA (24 ml, 3:1, v/v)  
32 was stirred at room overnight. The solvent was removed under reduced pressure, the  
33 residue was re-dissolved in DCM and the solvent was evaporated. This procedure was  
34 repeated several times.



1 The resulting oil was dried under *vacuum* to afford a white foam.  $^1\text{H}$  NMR ( $\text{CDCl}_3$ )  
2 revealed the disappearance of the signals assigned to the Boc groups on compound **6**.  
3 Quantitative deprotection was assumed. The residue (1.12 mmol, assuming quantitative  
4 deprotection) was dissolved in DCM (20 ml) and the solution was adjusted to pH 9-10  
5 (pH paper) by drop-wise addition of DIPEA. To this solution was added sequentially  
6 Lipoic acid (288 mg; 1.40 mmol), HOBT (214 mg; 1.40 mmol) and a solution of DCC  
7 (288 mg; 1.40 mmol) in DCM (5 ml). The solution was stirred at room temperature  
8 overnight. The DCU byproduct was removed by filtration and the reaction mixture was  
9 concentrated under reduced pressure. The residue was re-dissolved in ethyl acetate (100  
10 ml), and the solution was washed with  $\text{NaHCO}_3$  (50 ml, saturated solution) and brine  
11 (3x50 ml). The organic phase was dried ( $\text{MgSO}_4$ ) and concentrated under reduced  
12 pressure to afford the title compound (**7**) (358 mg; 44 %).  $^1\text{H}$  NMR (300 MHz,  $\text{CDCl}_3$ ):  
13  $\delta$ = 1.28 (m, 9 H,  $\text{C}(\text{O})\text{OCH}_2\text{CH}_3$ ), 1.48 (m, 2 H,  $\text{NHC}(\text{O})\text{CH}_2\text{CH}_2\text{CH}_2$ ), 1.70 (m, 2 H,  
14  $\text{NHC}(\text{O})\text{CH}_2\text{CH}_2$ ), 2.18 (m, 2 H,  $\text{NHC}(\text{O})\text{CH}_2\text{CH}_2\text{CH}_2\text{CH}_2$ ), 2.30 (m, 4 H,  $\text{NHC}(\text{O})\text{CH}_2$   
15 and  $\text{CHCH}_2\text{CH}_2\text{S}$ ), 2.60-3.60 (broad overlapped signals, integrating for 16 H,  
16  $\text{N}(\text{CH}_2)_2\text{N}$ ; 2 H, ABX; 2 H,  $\text{CHCH}_2\text{CH}_2\text{S}$ , 1 H,  $\text{CHSCH}_2\text{CH}_2\text{S}$ ), 3.73 (m, 6 H,  
17  $\text{C}(\text{O})\text{CH}_2\text{N}$ ), 3.97 (s, 3 H,  $\text{C}(\text{O})\text{OCH}_3$ ), 4.19 (m, 6 H,  $\text{C}(\text{O})\text{CH}_2\text{CH}_3$ ), 4.90 (dd, 1 H,  
18 ABX). HRMS (ESI):  $m/z$ : *ca.*cd. for  $\text{C}_{32}\text{H}_{58}\text{N}_5\text{O}_9\text{S}_2$   $[\text{M}+\text{H}]^+$ : 720.3676, found: 720.3645.  
19

20 **Preparation of ((5-(1,2-dithiolan-3-yl)-2-pentanamido)carboxyethyl)-4,7,10-tris-**  
21 **(carboxymethyl)-1,4,7,10-tetraazacyclododecane - fully deprotected DO3A-N-( $\alpha$ -**  
22 **lipoamido)propionate chelator (**L**<sub>1</sub>).**

23 Compound (**7**) (2.26 g, 3.15 mmol) was dissolved in a mixture water/ethanol (40 ml, 1/1  
24 v/v). The solution was adjusted to pH ~ 11 with aqueous NaOH 1 M (pH paper) and  
25 was left stirring at room temperature overnight. Then, the reaction mixture was adjusted  
26 to pH ~7 with hydrochloric acid 1 M (pH paper) and concentrated under reduced  
27 pressure. The residue was adsorbed onto silica and purified by flash chromatography  
28 ( $\text{CH}_2\text{Cl}_2 \rightarrow \text{CH}_2\text{Cl}_2/\text{EtOH}$  1/1  $\rightarrow \text{EtOH} \rightarrow \text{EtOH}/\text{H}_2\text{O}$  1/1  $\rightarrow \text{H}_2\text{O}$ ) to afford a light yellow  
29 foam. The final compound (**L**<sub>1</sub>) was further purified by size exclusion chromatography  
30 on Sephadex G10 (0.42  $\mu\text{m}$ ) with elution with water. The conductivity of the collected  
31 fractions was measured and were also tested by TLC (ethanol/water (1/1), revelation  
32 with iodine vapor). The high conductivity fractions (salt) were discarded and the  
33 medium/low conductivity fractions showing a signal on the TLC were pooled,  
34 concentrated at room temperature and further dried under vacuum to afford the final

1 deprotected compound as a light yellow solid (**L**<sub>1</sub>) (0.685 g, 35%). <sup>1</sup>H NMR (300 MHz,  
2 D<sub>2</sub>O): δ= 1.46 (m, *J*= 7.8 Hz, 2 H, NHC(O)CH<sub>2</sub>CH<sub>2</sub>CH<sub>2</sub>), 1.64-1.72 (m, 6 H,  
3 NHC(O)CH<sub>2</sub>CH<sub>2</sub>, NHC(O)CH<sub>2</sub>CH<sub>2</sub>CH<sub>2</sub>CH<sub>2</sub>, CHCH<sub>2</sub>CH<sub>2</sub>S), 2.01 (m, 2 H,  
4 NHC(O)CH<sub>2</sub>), 2.34 (t, *J*= 7.5 Hz 2 H, CHCH<sub>2</sub>CH<sub>2</sub>S), 2.49 (m, 1 H, CHSCH<sub>2</sub>CH<sub>2</sub>S),  
5 2.10-3.40 (broad overlapped signals integrating to 16 H, 4 x N(CH<sub>2</sub>)<sub>2</sub>N, 6 H, 3x  
6 NCH<sub>2</sub>C(O) and 2H, ABX), 4.49 (m, 1 H, ABX). <sup>13</sup>C NMR (75.4 MHz, D<sub>2</sub>O): 25.02 (1  
7 C, CH<sub>2</sub>), 28.32 (1 C, CH<sub>2</sub>), 33.93 (1 C, CH<sub>2</sub>), 35.73 (1 C, CH<sub>2</sub>), 38.22 (1 C, CH<sub>2</sub>), 40.46  
8 (2 C, 2xCH<sub>2</sub>), 47.81 (3 C, 3xCH<sub>2</sub>), 49.46 (1 C, CH<sub>2</sub>), 51.37 (1 C, CHCH<sub>2</sub>), 51.94 (2 C,  
9 CH<sub>2</sub>), 54.51 (2 C, CH<sub>2</sub>), 56.08 (2 C, CH<sub>2</sub>), 56.76 (2 C, CH<sub>2</sub>), 170.94 (1 C, C(O)), 176.65  
10 (2 C, 2xC(O)), 177.36 (2 C, 2xC(O)). HRMS (ESI): *m/z*: *calcd.* for C<sub>25</sub>H<sub>44</sub>N<sub>5</sub>O<sub>9</sub>S<sub>2</sub>  
11 [M+H]<sup>+</sup>: 622.2580, *found*: 622.2572.  
12

13 **Preparation of 11-mercaptoundecanoic acid conjugate DO3A-*N*-(α-**  
14 **mercaptoundecanamido)propionate - L<sub>2</sub>**

15  
16 **Synthesis of 11-(acetylthio)undecanoic acid (10)**

17  
18 To an ice-cooled solution of 11-mercaptoundecanoic acid (**9**) (2.00 g, 9.17 mmol) in  
19 pyridine (2.6 ml) was added acetic anhydride (2.6 ml, 2.81 g, 27.5 mmol). The solution  
20 was left stirring at room temperature overnight. Ice was directly added to the reaction  
21 mixture, followed by magnetic stirring until complete melting of the ice. The mixture  
22 was extracted with ethyl acetate (3×150 ml). The organic phase was washed with brine  
23 (3x30 ml), dried (MgSO<sub>4</sub>) and the solvent was removed under reduced pressure. The  
24 residue was further dried under vacuum to afford the final compound as an off-white  
25 solid (2.12 g, 89%). <sup>1</sup>H NMR (400 MHz, CDCl<sub>3</sub>): δ= 1.27 (s (*br*), 12 H, 6×CH<sub>2</sub>), 1.58-  
26 1.52 (m, 2 H, SCH<sub>2</sub>CH<sub>2</sub>), 1.66-1.59 (m, 2 H, (CO<sub>2</sub>H)CH<sub>2</sub>CH<sub>2</sub>), 2.32 (s, 3 H, C(O)CH<sub>3</sub>),  
27 2.35 (t, *J*= 7.2 Hz, 2 H, CH<sub>2</sub>COOH), 2.86 (t, *J*= 7.2 Hz, 2 H, SCH<sub>2</sub>). <sup>13</sup>C NMR (100.62  
28 MHz, CDCl<sub>3</sub>): δ= 24.61 (C(O)CH<sub>2</sub>CH<sub>2</sub>), 28.73 (SCH<sub>2</sub>), 28.97, 29.00, 29.10, 29.13,  
29 29.26, 29.32 (overlapped inner CH<sub>2</sub> signals), 29.43 (SCH<sub>2</sub>CH<sub>2</sub>), 30.59 (CH<sub>3</sub>), 33.99  
30 (C(O)CH<sub>2</sub>), 179.89 (COOH), 196.11 (SC(O)Me). HRMS (ESI): *m/z*: *calcd.* for  
31 C<sub>13</sub>H<sub>24</sub>NaO<sub>3</sub>S [M+Na]<sup>+</sup>: 283.1338, *found.*: 283.1339.  
32  
33  
34

1

2 **Synthesis of (11-(acetylthio)undecanoyl)serine methyl ester (11)**

3

4 To an ice-cooled solution of compound **10** (2.12 g, 8.14 mmol) in acetonitrile (70 ml)  
5 was added HOBt (1.85 g, 8.95 mmol) and a solution of DCC (1.25 g, 8.14 mmol) in  
6 acetonitrile (10 ml). The mixture was left stirring at the ice bath temperature and after  
7 15 minutes L-serine methyl ester hydrochloride (1.27 g, 8.14 mmol) and triethylamine  
8 (1.13 ml, 0.82 g, 8.14 mmol) were added. The reaction mixture was left stirring at room  
9 temperature overnight. The DCU byproduct was removed by filtration and the sample  
10 was concentrated under reduced pressure. The residue was re-dissolved in ethyl acetate  
11 (100 ml) and the solution was washed sequentially with KHSO<sub>4</sub> (1 M, 3x50 ml),  
12 NaHCO<sub>3</sub> (saturated solution, 50 ml) and brine (3x50 ml). The organic phase was dried  
13 (MgSO<sub>4</sub>) and concentrated under reduced pressure to afford title compound **11** (2.73 g;  
14 93%). <sup>1</sup>H-NMR (CDCl<sub>3</sub>, 400 MHz): δ= 1.25 (s (*br*), 12 H, 6 × CH<sub>2</sub>), 1.52-1.57 (m, 2 H,  
15 SCH<sub>2</sub>CH<sub>2</sub>), 1.58-1.65 (m, 2 H, NHC(O)CH<sub>2</sub>CH<sub>2</sub>), 2.25 (t, *J*= 7.2 Hz, 2 H,  
16 NHC(O)CH<sub>2</sub>), 2.30 (s, 3 H, SC(O)CH<sub>3</sub>), 2.84 (t, *J*= 7.2 Hz, 2 H, SCH<sub>2</sub>), 3.76 (s, 3 H,  
17 OCH<sub>3</sub>), 3.87 (ddd, *J*= 3.6, 11.2, 29.8 Hz, 1 H, CH<sub>a</sub>H<sub>b</sub>OH), 3.96 (ddd, *J*= 4.0, 11.0 and  
18 29.8 Hz, 1 H, CH<sub>a</sub>H<sub>b</sub>OH), 4.67-4.63 (m, 1 H, CH), 6.62 (s (*br*), 1 H, NH). <sup>13</sup>C-NMR  
19 (CDCl<sub>3</sub>, 100.62 MHz): δ= 24.80 (NHC(O)CH<sub>2</sub>CH<sub>2</sub>), 28.67, 28.95, 29.06, 29.09  
20 (overlapped CH<sub>2</sub> signals), 29.17 (SCH<sub>2</sub>), 29.25, 29.27 (overlapped CH<sub>2</sub> signals), 29.37  
21 (SCH<sub>2</sub>CH<sub>2</sub>), 30.55 (SC(O)Me), 36.37 (C(O)CH<sub>2</sub>), 52.54 (OMe), 54.54 (CH), 63.20  
22 (CH<sub>2</sub>OH), 171.03 (C(O)OMe), 173.78 (NHC(O)), 196.19 (SC(O)).

1 **Synthesis of *N*-(*tert*-butoxycarbonyl),*N*-(11-(acetylthio)undecanoyl)**  
2 **dehydroalanine methyl ester (3)**

3

4 To a solution of compound (11) (0.866 g, 2.40 mmol) in dry acetonitrile (15 ml) was  
5 sequentially added DMAP (0.081 g, 0.66 mmol) and Boc<sub>2</sub>O (1.44 g, 6.6 mmol). The  
6 mixture was left stirring for 5 days at room temperature. The reaction progress was  
7 monitored by <sup>1</sup>H NMR. A small volume of reaction mixture was removed, worked-up  
8 was as described below, and analyzed by <sup>1</sup>H NMR by monitoring the disappearance of  
9 the signal of the intermediate carbonate ester and the appearance of the alkenic signals  
10 at δ= 5.62 and 6.44 ppm. The solid residues were removed by filtration and the sample  
11 was concentrated under reduce pressure. The residue was re-dissolved in ethyl acetate  
12 (150 ml), and the solution was washed sequentially with KHSO<sub>4</sub> (1 M, 3x50 ml),  
13 NaHCO<sub>3</sub> (saturated solution, 50 ml) and brine (3x50 cm<sup>3</sup>). The organic phase was  
14 concentrated under reduced pressure and the residue was purified by a flash  
15 chromatography (*n*-hexane→*n*-hexane/ethyl acetate (70:30)) to afford the title  
16 compound as a thick reddish oil (0.445 g, 58%). <sup>1</sup>H-NMR (CDCl<sub>3</sub>, 400 MHz) δ= 1.27 (s  
17 (*br*), 12 H, 6×CH<sub>2</sub>), 1.46 (s, 9 H, C(CH<sub>3</sub>)<sub>3</sub>), 1.49-1.57 (m, 2 H, SCH<sub>2</sub>CH<sub>2</sub>), 1.65 (m, 2 H,  
18 C(O)CH<sub>2</sub>CH<sub>2</sub>), 2.32 (s, 3 H, SC(O)CH<sub>3</sub>), 2.86 (t, *J*= 7.6 Hz, 2 H, NHC(O)CH<sub>2</sub>), 2.93  
19 (t, *J*= 7.6 Hz, 2 H, SCH<sub>2</sub>), 3.78 (s, 3 H, C(O)OCH<sub>3</sub>), 5.62 (s, 1 H, CCH<sub>a</sub>H<sub>b</sub>), 6.44 (s, 1  
20 H, CCH<sub>a</sub>H<sub>b</sub>). <sup>13</sup>C-NMR (CDCl<sub>3</sub>, 100.62 MHz): δ= 24.71 (C(O)CH<sub>2</sub>CH<sub>2</sub>), 27.40  
21 (SCH<sub>2</sub>CH<sub>2</sub>), 27.80 (3×OCCH<sub>3</sub>), 28.75, 29.05, 29.08, 29.11, 29.35, 29.44 (overlapped  
22 CH<sub>2</sub> signals), 29.38 (C(O)CH<sub>2</sub>), 30.59 (SC(O)CH<sub>3</sub>), 37.66 (SCH<sub>2</sub>), 52.38 (C(O)OCH<sub>3</sub>),  
23 83.53 (OCCH<sub>3</sub>), 125.71 (CCH<sub>2</sub>), 135.56 (CCH<sub>2</sub>), 151.52 (NC(O)O), 163.68  
24 (C(O)OCH<sub>3</sub>), 175.66 (NC(O)), 196.00 (SC(O)). HRMS (ESI): *m/z*: calcd. for  
25 C<sub>22</sub>H<sub>37</sub>NaO<sub>6</sub>S [M+Na]<sup>+</sup>: 466.2234, found: 466.2223.

26

27 **Synthesis of (11-(acetylthio)-2-*N*-(*tert*-butoxycarbonyl)undecanamido-**  
28 **methoxycarbonylethyl)-1,4,7,10-tetraazacyclododecane - monoalkylated cyclen (5)**

29

30 To a solution of *cyclen* (0.260 g, 1.5 mmol) in acetonitrile (30 ml) was added K<sub>2</sub>CO<sub>3</sub>  
31 (0.83 g, 6.0 mmol) and in several portions compound 3 (0.445 g, 1.0 mmol). The  
32 suspension was vigorously stirred at room temperature for 4 hours. The suspended solid  
33 was removed by filtration and the solvent was evaporated under reduced pressure.

34

1 The residue was purified by flash chromatography  
2 ( $\text{CH}_2\text{Cl}_2 \rightarrow \text{CH}_2\text{Cl}_2/\text{EtOH}/\text{NH}_3/\text{H}_2\text{O}$  (70:30:5:5)) to afford the title compound **5** as a  
3 white foam (0.451 g, 73.0 %).  $^1\text{H-NMR}$  ( $\text{CDCl}_3$ , 400 MHz):  $\delta$  = 1.33 (s (*br*), 12 H,  
4  $6 \times \text{CH}_2$ ), 1.47 (s, 9 H,  $\text{OC}(\text{CH}_3)_3$ ), 1.60 (m, 2 H,  $\text{C}(\text{O})\text{CH}_2\text{CH}_2$ ), 1.60-1.65 (m, 2 H,  
5  $\text{SCH}_2\text{CH}_2$ ), 2.33 (s, 3 H,  $\text{SC}(\text{O})\text{CH}_3$ ), 2.51-2.65 (m, 16 H,  $4 \times \text{N}(\text{CH}_2)_2\text{N}$ ), 2.74-2.79 (m,  
6 2 H, ( $\text{NHC}(\text{O})\text{CH}_2$ )), 2.74-2.79 (m, 1 H,  $\text{NCH}_a\text{CH}_b\text{CH}$ ), 2.85 (t,  $J$  = 7.2 Hz, 2 H,  
7  $\text{CH}_3\text{C}(\text{O})\text{SCH}_2$ ), 3.45 (dd,  $J$  = 5.2 and 14.4 Hz, 1 H,  $\text{NCH}_a\text{CH}_b\text{CH}$ ), 3.68 (s, 3 H,  
8  $\text{C}(\text{O})\text{OCH}_3$ ), 5.46 (t,  $J$  = 5.2 Hz, 1 H,  $\text{NCH}_2\text{CH}$ ).  $^{13}\text{C-NMR}$  ( $\text{CDCl}_3$ , 100.62 MHz):  $\delta$  =  
9 25.01 ( $\text{C}(\text{O})\text{CH}_2\text{CH}_2$ ), 27.90 ( $\text{OCCH}_3$ ), 28.75 ( $\text{SCH}_2$ ), 29.05, 29.10, 29.17, 29.37, 29.39,  
10 29.40 (overlapped  $\text{CH}_2$  signals), 29.43 ( $\text{SCH}_2\text{CH}_2$ ), 30.58 ( $\text{SC}(\text{O})\text{Me}$ ), 40.06  
11 ( $\text{C}(\text{O})\text{CH}_2$ ), 46.92 ( $6 \times \text{NHCH}_2$ ), 51.07 ( $2 \times \text{CH}_2\text{NCH}_2\text{CH}$ ), 52.16 ( $\text{C}(\text{O})\text{OMe}$ ), 53.56  
12 ( $\text{NCH}_2\text{CH}$ ), 58.06 ( $\text{NCH}_2\text{CH}$ ), 83.99 (C), 151.96 ( $\text{NC}(\text{O})\text{O}$ ), 170.84 ( $\text{C}(\text{O})\text{OMe}$ ),  
13 175.52 ( $\text{N}(\text{Boc})\text{C}(\text{O})\text{CH}_2$ ), 195.99 ( $\text{SC}(\text{O})$ ). HRMS (ESI):  $m/z$ : calcd. for  $\text{C}_{30}\text{H}_{58}\text{N}_5\text{O}_6\text{S}$   
14  $[\text{M}+\text{H}]^+$ : 616.4102, found.: 616.4100.

15

16 **Synthesis of (11-(acetylthio)-2-undecanamido-methoxycarbonylethyl)-4,7,10-**  
17 **tris-(ethoxycarbonylmethyl)-1,4,7,10-tetraazacyclododecane - fully alkylated cyclen**  
18 **(8)**

19

20 A solution of monoalkylated cyclen **5** (0.451 g, 0.87 mmol) in trifluoroacetic acid in  
21 dichlorometane (33%, 24 ml) was stirred overnight at room temperature. The solvent  
22 was evaporated at reduced pressure and the residue was re-dissolved in dichlorometane.  
23 The solvent was evaporated again, and this procedure was repeated several times to give  
24 a light thick yellow oil which was further dried under vacuum.  $^1\text{H NMR}$  spectroscopy  
25 ( $\text{CDCl}_3$ ) revealed the disappearance of the signal assigned to the Boc group in the  
26 precursor compound **5**. The deprotected compound (0.87 mmol, assuming quantitative  
27 deprotection) was re-dissolved in MeCN (20 ml),  $\text{K}_2\text{CO}_3$  (1.17 g, 8.46 mmol) was  
28 added and the suspension was left under vigorous stirring at room temperature for 30  
29 minutes. Ethyl bromoacetate (0.29 ml, 2.61 mmol) was added, and the suspension was  
30 further stirred for 2 hours. The suspended solids were removed by filtration, the solvent  
31 was evaporated under reduce pressure and the residue was purified by flash  
32 chromatography ( $\text{CH}_2\text{Cl}_2 \rightarrow \text{CH}_2\text{Cl}_2/\text{EtOH}$  (7:3)) to afford compound **8** (0.218 g, 32 %)  
33 as a white foam.

1 <sup>1</sup>H-NMR (CDCl<sub>3</sub>, 400 MHz): δ= 1.33 (m, 12 H, 6×CH<sub>2</sub>), 1.47 (s, 9 H, OC(CH<sub>3</sub>)<sub>3</sub>), 1.60  
2 (m, 2 H, C(O)CH<sub>2</sub>CH<sub>2</sub>), 1.60-1.65 (m, 2 H, SCH<sub>2</sub>CH<sub>2</sub>), 2.32 (s, 3 H, SC(O)Me), 2.70-  
3 2.90 (m, 16 H, 4×N(CH<sub>2</sub>)<sub>2</sub>N), 2.74-2.79 (m, 2 H, (C(O)CH<sub>2</sub>)), 2.74-2.79 (m, 1 H,  
4 NCH<sub>3</sub>CH<sub>b</sub>CH), 2.85 (t, *J*= 7.2 Hz, 2 H, SCH<sub>2</sub>), 3.49 (m, 6 H, 3×C(O)CH<sub>2</sub>CH<sub>3</sub> and 1 H,  
5 NCH<sub>d</sub>CH<sub>b</sub>CH), 3.72 (s, 3 H, C(O)OCH<sub>3</sub>), 4.19 (m, 6 H, C(O)OCH<sub>2</sub>CH<sub>3</sub>), 5.46 (t, *J*= 5.2  
6 Hz, 1 H, NCH<sub>2</sub>CH). HRMS (ESI): *m/z*: calcd. for C<sub>37</sub>H<sub>68</sub>N<sub>5</sub>O<sub>10</sub>S [M+H]<sup>+</sup>: 774.4681,  
7 found: 774.4684.

8

9

10

11

12

13

14

15

16

17

18

19

20

21

22

23

24

25

26

27

28

1 **Synthesis of (11-mercapto-2-undecanamido-carboxyethyl)-4,7,10-tris-**  
2 **(carboxymethyl)-1,4,7,10-tetraazacyclododecane - Fully deprotected DO3A-N-( $\alpha$ -**  
3 **mercaptoundecanamido)propionate chelator (L<sub>2</sub>)**

4 Compound **8** (0.218 g, 0.28 mmol) was dissolved in a mixture EtOH/H<sub>2</sub>O (20 ml, 1:1  
5 (v/v)). The solution was adjusted to pH ~ 10-11 (pH paper) with aqueous NaOH (1 M)  
6 and left stirring at room temperature overnight. The solution was adjusted to pH ~ 7 (pH  
7 paper) with diluted hydrochloric acid (1M) and was evaporated at reduced pressure  
8 (temperature < 40 °C). The residue was adsorbed onto silica and purified by flash  
9 chromatography (CH<sub>2</sub>Cl<sub>2</sub> → CH<sub>2</sub>Cl<sub>2</sub>/EtOH 1/1 → EtOH → EtOH/H<sub>2</sub>O 1:1 → H<sub>2</sub>O) to afford  
10 a light yellow foam. The residue was re-dissolved in water and was purified by size  
11 exclusion chromatography (Sephadex G10). The relevant fractions were pooled together  
12 and the solvent was removed under reduced pressure to give chelator **L<sub>2</sub>** (0.074 g, 42  
13 %). <sup>1</sup>H-NMR (CDCl<sub>3</sub>, 400 MHz):  $\delta$ = 1.33 (s (*br*), 10 H, 5×CH<sub>2</sub>), 1.61 (s (*br*), 2 H,  
14 SCH<sub>2</sub>CH<sub>2</sub>CH<sub>2</sub>), 1.63 (s (*br*), 2 H, (C(O)CH<sub>2</sub>CH<sub>2</sub>), 1.72 (s (*br*), 2 H, SCH<sub>2</sub>CH<sub>2</sub>), 2.33 (s  
15 (*br*), 2 H, (C(O)CH<sub>2</sub>), 2.58 (t, *J*= 6.8 Hz, 2 H, SCH<sub>2</sub>), 2.80 (s (*br*), 1 H, NCH<sub>a</sub>H<sub>b</sub>CH),  
16 2.80 (s (*br*), 1 H, NCH<sub>a</sub>H<sub>b</sub>CH), 3.18 (s, 4 H, NCH<sub>2</sub>CH<sub>2</sub>NCH<sub>2</sub>CH), 3.39-3.36 (m, 4 H,  
17 N(CH<sub>2</sub>)<sub>2</sub>N), 3.43 (s, 8 H, 2×N(CH<sub>2</sub>)<sub>2</sub>N), 3.76 (s (*br*), 6 H, 3×NCH<sub>2</sub>(C(O)OH), 4.52 (s  
18 (*br*), 1 H, CH). <sup>13</sup>C-NMR (CDCl<sub>3</sub>, 100.62 MHz):  $\delta$ = 23.82 (SCH<sub>2</sub>), 25.13  
19 (C(O)CH<sub>2</sub>CH<sub>2</sub>), 27.73 (SCH<sub>2</sub>CH<sub>2</sub>), 28.11, 28.31, 28.39, 28.52, 28.61 (overlapped CH<sub>2</sub>  
20 signals), 33.08 (SCH<sub>2</sub>CH<sub>2</sub>CH<sub>2</sub>), 35.84 (C(O)CH<sub>2</sub>), 38.51 (NCH<sub>2</sub>CH), 48.79 (2×  
21 NCH<sub>2</sub>CH<sub>2</sub>NCH<sub>2</sub>CH), 51.20 (CH), 51.62 (2×NCH<sub>2</sub>CH<sub>2</sub>NCH<sub>2</sub>CH), 56.56 (3×  
22 NCH<sub>2</sub>(C(O)OH), 56.09 (2×NCH<sub>2</sub>CH<sub>2</sub>N), 177.14 (NHC(O)), 177.14 (CHC(O)OH),  
23 177.30 (3×NCH<sub>2</sub>C(O)OH). HRMS (ESI): *m/z*: calcd for C<sub>28</sub>H<sub>51</sub>N<sub>5</sub>NaO<sub>9</sub>S [M+Na]<sup>+</sup>:  
24 656.3305, found: 656.3300.

25

26 **Preparation of GdL<sub>1</sub> and GdL<sub>2</sub> complexes for relaxometric measurements**

27

28 A solution of GdCl<sub>3</sub>.6H<sub>2</sub>O was added drop-wise, under magnetic stirring, to an  
29 equimolar solution of **L<sub>1</sub>** or **L<sub>2</sub>** (5% excess), while keeping the solution pH around 5.8  
30 (pH meter) by the addition of diluted NaOH. The solution was left stirring at room  
31 temperature overnight. Then, the solution was adjusted to pH 7.0 with NaOH (0.1 M)  
32 and filtered through a 0.2  $\mu$ m syringe filter. The absence of free Gd<sup>3+</sup> was confirmed by  
33 the xylenol orange test. The final concentration of Gd was determined by ICP-OES  
34 following sample digestion with nitric acid.

1

2 **Preparation gold nanoparticles functionalized with GdL<sub>1</sub> and GdL<sub>2</sub> chelates.**

3

4 An aqueous solution of ligand DO3A-*N*-( $\alpha$ -Lipoamido)propionate (**L<sub>1</sub>**) (20.5 mM, 4.53  
5 ml, 0.091 mmol) was added drop-wise, under magnetic stirring at room temperature, to  
6 an aqueous solution of HAuCl<sub>4</sub> (58.86 mM, 1.54 ml, 0.091 mmol). During the initial  
7 stages of the addition of **L<sub>1</sub>**, the light yellow HAuCl<sub>4</sub> solution turned dark orange,  
8 fading away in color to light yellow with further addition of ligand. To the reaction  
9 mixture was added, in one aliquot, a freshly prepared aqueous NaBH<sub>4</sub> solution (522  
10 mM, 0.179 ml, 0.093 mmol). The reaction mixture turned instantaneously dark brown  
11 and was left stirring at room temperature for 16 hours. The NPs solution was adjusted to  
12 pH  $\sim$  7 (pH meter) by adding aqueous NaOH (0.1 M) and was filtered through a 0.20  
13  $\mu$ m PTFE syringe filter. A small volume of solution (1 ml) was kept for further  
14 characterization. To remaining NPs solution ( $\sim$  5.3 ml) was added slowly a solution of  
15 GdCl<sub>3</sub>.6H<sub>2</sub>O in water (303  $\mu$ M, 0.300 ml, 0.091 mmol) while keeping the solution pH  
16 around 5.5 (pH meter) by adding aqueous NaOH 0.1 M. The NPs solution was left  
17 stirring at room temperature for 16 hours and was adjusted to pH  $\sim$  7 with aqueous  
18 NaOH (1 M solution). The nanoparticles were purified by size exclusion  
19 chromatography (Sephadex G10, 0.42  $\mu$ m) with elution with water. The entire colored  
20 broad band eluting from the column was collected without attempting to fractionate the  
21 sample. The nanoparticles were further purified by extensive dialysis against water  
22 using a 10 KDa MWCO cellulose membrane. The xylenol orange test indicated the  
23 absence of free Gd<sup>3+</sup> in the gold nanoparticles preparation.

24 The same procedure was followed for the preparation of GdL<sub>2</sub>@AuNPs starting  
25 from ligand **L<sub>2</sub>** (20.5 mg/mL, 2 ml, 0.0647 mmol) and HAuCl<sub>4</sub> (22 mg/ml, 1 ml, 0.0647  
26 mmol).

27 The Gd and Au content of the NPs preparations ([Gd]= 0.57 mM and 1.30 mM;  
28 [Au]/[Gd]= 1.40 and 0.87, for GdL<sub>1</sub>@AuNPs and GdL<sub>2</sub>@AuNPs, respectively) was  
29 determined by ICP-OES analysis following sample digestion with *aqua regia*.

30

31 **NMRD measurements**

32



1 The NMD measurements were performed using a StelarSpinmaster FFC NMR  
2 relaxometer (0.01-20 MHz) equipped with a VTC90 temperature control unit. At higher  
3 fields, the  $^1\text{H}$  relaxivity measurements were performed on Bruker Minispecs mq30 (30  
4 MHz), mq40 (40 MHz) and mq60 (60 MHz), as well as Bruker Advance spectrometers  
5 connected to 2.35 T, 4.7 T and 9.4 T superconducting magnets. In each case, the  
6 temperature was measured by a substitution technique. Variable temperature  
7 measurements were performed at 25 and 37 °C. The NMRD profiles were analysed  
8 using the Visualiseur/Optimiseur 3.6 program running on a Matlab® 6.5 platform.<sup>49</sup>

### 10 **Relaxivity studies of pH dependence and $\text{Zn}^{2+}$ transmetallation**

11  
12 The transmetallation reaction of the  $\text{GdL}_1$  and  $\text{GdL}_2$  chelates and of the metal chelate-  
13 decorated NPs  $\text{GdL}_1@AuNPs$  and  $\text{GdL}_2@AuNPs$  against  $\text{Zn}^{2+}$ , was studied by  
14 following the time-dependent decrease of the protonic longitudinal relaxation rate,  $R_1$ ,  
15 (20 MHz, 25 °C) of phosphate-buffered saline solutions (PBS, pH 7.1, 10 mM),  
16 containing  $\text{GdL}_1$ ,  $\text{GdL}_2$ ,  $\text{GdL}_1@AuNPs$  and  $\text{GdL}_2@AuNPs$  ( $[\text{Gd}] = 1.0, 1.13, 0.42, 1.33$   
17 mM, respectively), before and after adding an equimolar amount of  $\text{ZnCl}_2$ , while  
18 vigorously stirring the solutions.

19 The pH dependence of the relaxivity was measured by adjusting the solution pH  
20 with aqueous diluted NaOH (0.1 M) or diluted hydrochloric acid (0.1 M), using a  
21 Crison micro TT 2050 pH meter equipped with a Mettler Toledo 422 electrode. A  
22 Bruker Minispec mq20 relaxometer was used for all measurements (20 MHz, 25 °C).

### 24 **MRI studies**

#### 26 **Preparation of the $\text{GdL}_1@AuNPs$ and $\text{GdL}_2@AuNPs$ CA solutions for MRI 27 studies.**

28  
29 The  $\text{GdL}_1@AuNPs$  and  $\text{GdL}_2@AuNPs$  CA for the MRI studies were prepared  
30 following the procedure described above. The final nanoparticles solutions were freeze-  
31 dried and their Gd and Au content (per mg of solid material) were determined by ICP-  
32 OES following digestion with *aqua regia*.

1 ***In vivo* MRI studies.**

2

3 The experimental protocols were approved by the appropriate institutional review  
4 committees and meet the guidelines of their responsible governmental agency. The  
5 Magnetic Resonance Imaging (MRI) experiments were all performed on a Bruker  
6 Pharmascan platform (Bruker Medical GmbH, Ettlingen, Germany) using a 7.0 T (300  
7 MHz) horizontal-bore superconducting magnet, equipped with a  $^1\text{H}$  selective 60 mm  
8 birdcage resonator and a Bruker gradient insert with 90 mm diameter (maximum  
9 intensity 360 mT/m). Data were acquired using a Hewlett-Packard console running  
10 Paravision software (Bruker Medical GmbH, Ettlingen, Germany) under a LINUX  
11 environment.

12 All MRI examinations were carried out on mice ( $n = 4$ ,  $\sim 20$  g body weight)  
13 anaesthetized initially by inhalation in an induction box with  $\text{O}_2$  (1 L/min) containing 3  
14 % isoflurane, and maintained during the experiment using a face mask allowing free  
15 breathing and 1-2 % isoflurane on  $\text{O}_2$ . Animals were taped down into a holder, to  
16 minimize breathing - related motion, and were then placed in a heated probe, which  
17 maintained the core body temperature at  $37 \pm 0.5$  °C, monitored by a rectal probe. The  
18 physiological state of the animal was monitored throughout the entire experiment by a  
19 Biotrig physiological monitor (Bruker Medical GmbH, Ettlingen, Germany), using the  
20 respiratory rate and body temperature.

21 Solutions of  $\text{GdL}_1@Au\text{NPs}$  and  $\text{GdL}_2@Au\text{NPs}$  10 mM in [Gd] were prepared  
22 by dissolving the freeze-dried NPs in the appropriate volume of PBS buffer. The  
23 solutions were filtered through a 0.2  $\mu\text{m}$  syringe filter before injection. 10 mM  
24 Gd(DTPA) (Magnevist<sup>®</sup>, Schering, Berlin, Germany) solutions were also prepared. The  
25 solutions were injected into the catheterized tail vein as a bolus in 20 s (0.05 and 0.1  
26 mmol Gd  $\text{kg}^{-1}$  body weight) using an infusion pump (Panlab, Barcelona, Spain).

27 Regional contrast agent uptake was assessed using Dynamic Contrast Enhanced  
28 (DCE) MRI. DCE MRI experiments were performed with series of  $T_1$ -weighted spin  
29 echo images sequentially acquired over 1 h, before and following the injection of the  
30 contrast agent 10 min after the beginning of the study. The acquisition parameters were:  
31  $\text{TR} = 310$  ms,  $\text{TE} = 10.58$  ms, number of averages = 2, ten coronal slices, slice thickness  
32 = 2 mm,  $\text{FOV} = 5.0 \times 5.0$  cm, matrix = 256 x 256, 30 repetitions with a total acquisition  
33 time of 119 s.

34

## 1 **MRI data analysis.**

2

3 Data were analyzed with the public domain software Image J (<http://rsbweb.nih.gov/ij/>).  
4 With the aim of comparing the pharmacokinetics obtained from different animals, the  
5 data were normalized by calculating the percentage of relative, rather than absolute,  
6 enhancement:

$$7 \quad RE = \frac{(I - I_0)}{I_0} \times 100$$

8 where  $I$  is the signal intensity at any given time after CA injection and  $I_0$  is the intensity  
9 before injection. Pharmacokinetic behaviour was analyzed by calculating the average  
10 enhancements within the different regions of interest (ROIs) placed on each one of the  
11 following regions: liver, kidney medulla, kidney cortex and muscle.

12

## 13 **Biodistribution of radiolabeled nanoparticles**

14

### 15 **Preparation of [ $^{153}\text{Sm}$ ]L<sub>1</sub>@AuNPs chelates for the biodistribution studies**

16

17 In these studies  $^{153}\text{Sm}^{3+}$  was used as a radioactive surrogate of  $\text{Gd}^{3+}$ . [ $^{153}\text{SmCl}_3$ ] (1 mCi)  
18 was added to a solution of L<sub>1</sub>@AuNPs (5 mg freeze-dried NPs) in sodium acetate buffer  
19 (400  $\mu\text{L}$ , 0.4 M, pH 5). The solution was stirred at 80 °C for 5 hours. After that, cold  
20  $\text{SmCl}_3$  was added to each solution in order to obtain an equimolar  $\text{Sm}^{3+}$ :chelator ratio.  
21 The final solution was heated at 80 °C for 2 hours and left overnight at room  
22 temperature. The radiolabeled nanoparticles were purified by size exclusion  
23 chromatography using a Sephadex G-10 column eluted with 0.4 M acetate buffer. The  
24 whole colored broad band eluting from the column was collected and concentrated by  
25 centrifugal filtration (Centricon 10 kDa MWCO membrane, Millipore).

26

## 27 **Biodistribution studies**

28

29 Groups of four animals (Wistar rat males weighting ca 200 g) were anaesthetized with  
30 Ketamine (50.0 mg/mL)/chlorpromazine (2.5%) (10:3) and injected in the femoral vein  
31 with ca 100  $\mu\text{Ci}$  of [ $^{153}\text{Sm}$ ]L<sub>1</sub>@AuNPs and sacrificed 2 and 24 hours later. The major  
32 organs were excised, weighed and the tissue radioactivity was measured in a  $\gamma$  well-

1 counter. Blood samples were obtained at appropriate periods of time, weighted and  
2 radioactivity counted.

3 National regulations for the care and use of laboratory animals were strictly followed in  
4 this study.

### 6 **Semiempirical calculations, molecular modelling and NPs size estimates**

7  
8 All calculations were performed with Mopac code<sup>50</sup> using the semiempirical model  
9 Hamiltonian PM6<sup>51</sup> and COSMO<sup>52</sup> implicit water solvent model ( $\epsilon=74.8$  with Gd and  
10 Au tesserae radius taken as 0.2 nm). The length of the chelates was estimated from  
11 various chelate conformers averaged over several S...O and S...H top bottom distances  
12 within conformers (Figure SI5); ascribing an error of 0.1 nm to the estimates seems  
13 reasonable for this methodology. The average AuNPs diameter is estimated from the  
14 diameter exclusion of the left and right chelates (Table SI2).

### 17 **Acknowledgements**

18  
19 This work was financially supported by Fundação para a Ciência e a Tecnologia,  
20 Portugal: PhD grant SFRH/BD/63994/2009 to Miguel Ferreira and Sabbatical Grant  
21 SFRH/BSAB/1328/2013 to José Martins at Bath University, UK; and Rede Nacional de  
22 NMR (REDE/1517/RMN/2005) for the acquisition of the Varian VNMRS 600 NMR  
23 spectrometer in Coimbra. T.B.R. was supported by a Marie Curie Fellowship (FP/-  
24 PEOPLE-2009-IEF 254380) and an EMBO Fellowship (ALTF 1145-2009). Financial  
25 support from Ministerio de Ciencia e Innovación, Spain, projects SAF2011-23622  
26 (S.C.) and CTQ2010-20960-C02-02 (P.L.-L.), and Comunidad de Madrid, Spain,  
27 project S2010/BMD-2349 (S.C. and P.L.-L.), is also acknowledged. B. Mousavi and L.  
28 Helm acknowledge financial support by the Swiss National Science Foundation. This  
29 work was carried out in the frame of the COST D38 Action “Metal Based Systems for  
30 Molecular Imaging” and COST TD1004 Action “Theranostics Imaging and Therapy”.

31  
32  
33  
34

1

2 **References**

- 3 1. M. L. James and S. S. Gambhir, *Physiol. Reviews*, 2012, **92**, 897-965.
- 4 2. G. J. Stanis, E. E. Odrobina, J. Pun, M. Escaravage, S. J. Graham, M. J.  
5 Bronskill and R. M. Henkelman, *Magn. Reson. Med.*, 2005, **54**, 507-512.
- 6 3. S. Laus, R. Ruloff, E. Toth and A. E. Merbach, *Chem. Eur. J.*, 2003, **9**, 3555-  
7 3566.
- 8 4. P. Caravan, J. J. Ellison, T. J. McMurry and R. B. Lauffer, *Chem. Rev.*, 1999,  
9 **99**, 2293-2352.
- 10 5. E. M. Gale, S. Mukherjee, C. Liu, G. S. Loving and P. Caravan, *Inorg. Chem.*,  
11 2014, **53**, 10748-10761.
- 12 6. E. Tanimoto, S. Karasawa, S. Ueki, N. Nitta, I. Aoki and N. Koga, *RSC*  
13 *Advances*, 2013, **3**, 3531-3534.
- 14 7. B.-T. Doan, S. Meme and J.-C. Beloeil, in *The Chemistry of Contrast Agents in*  
15 *Medical Magnetic Resonance Imaging*, John Wiley & Sons, Ltd, 2013, pp. 1-23.
- 16 8. G. J. Strijkers, W. J. Mulder, G. A. van Tilborg and K. Nicolay, *Anti-cancer*  
17 *Agents Med. Chem.*, 2007, **7**, 291-305.
- 18 9. Y. X. Wang, *Quant. imaging Med. Surgery*, 2011, **1**, 35-40.
- 19 10. Z. Zhou and Z. R. Lu, *Wiley interdiscip. Rev. Nanomed nanobiotechnol.*, 2013,  
20 **5**, 1-18.
- 21 11. J. E. Rosen, S. Yoffe, A. Meerasa, M. Verma, F. X. Gu, *J. Nanomedic.*  
22 *Nanotechnol.*, 2011, **2**, 115.
- 23 12. X. Ding, C. H. Liow, M. Zhang, R. Huang, C. Li, H. Shen, M. Liu, Y. Zou, N.  
24 Gao, Z. Zhang, Y. Li, Q. Wang, S. Li and J. Jiang, *J. Am. Chem. Soc.*, 2014,  
25 **136**, 15684-15693.
- 26 13. D. K. Chatterjee, P. Diagaradjane and S. Krishnan, *Ther. deliv.*, 2011, **2**, 1001-  
27 1014.
- 28 14. N. Khlebtsov and L. Dykman, *Chem Soc Rev*, 2011, **40**, 1647-1671.
- 29 15. Y. Zhang, W. Chu, A. Foroushani, H. Wang, D. Li, J. Liu, C. Barrow, X. Wang  
30 and W. Yang, *Materials*, 2014, **7**, 5169-5201.
- 31 16. C. Alric, J. Taleb, G. L. Duc, C. Mandon, C. Billotey, A. L. Meur-Herland, T.  
32 Brochard, F. Vocanson, M. Janier, P. Perriat, S. Roux and O. Tillement, *J. Am.*  
33 *Chem. Soc.*, 2008, **130**, 5908-5915.
- 34 17. P. J. Debouttière, S. Roux, F. Vocanson, C. Billotey, O. Beuf, A. Favre-  
35 Réguillon, Y. Lin, S. Pellet-Rostaing, R. Lamartine, P. Perriat and O. Tillement,  
36 *Adv. Funct. Mat.*, 2006, **16**, 2330-2339.
- 37 18. J. A. Park, P. A. N. Reddy, H. K. Kim, I. S. Kim, G. C. Kim, Y. Chang and T. J.  
38 Kim, *Bioorg. & Med. Chem. Lett.*, 2008, **18**, 6135-6137.
- 39 19. M. Marradi, D. Alcantara, J. M. de la Fuente, M. L. Garcia-Martin, S. Cerdan  
40 and S. Penades, *Chem. Comm.*, 2009, 3922-3924.
- 41 20. I. Miladi, C. Alric, S. Dufort, P. Mowat, A. Dutour, C. Mandon, G. Laurent, E.  
42 Bräuer-Krisch, N. Herath, J.-L. Coll, M. Dutreix, F. Lux, R. Bazzi, C. Billotey,  
43 M. Janier, P. Perriat, G. Le Duc, S. Roux and O. Tillement, *Small*, 2014, **10**,  
44 1116-1124.
- 45 21. M. F. Warsi, R. W. Adams, S. B. Duckett and V. Chechik, *Chem. Comm.*, 2010,  
46 **46**, 451-453.
- 47 22. M. F. Warsi and V. Chechik, *Phys. Chem. Chem. Phys.*, 2011, **13**, 9812-9817.
- 48 23. L. c. Moriggi, C. Cannizzo, E. Dumas, C. d. R. Mayer, A. Ulianov and L. Helm,  
49 *J. Am. Chem. Soc.*, 2009, **131**, 10828-10829.

- 1 24. M. F. Ferreira, A. F. Martins, J. A. Martins, P. M. Ferreira, E. Toth and C.  
2 Geraldes, *Chem. Comm.*, 2009, 6475-6477.
- 3 25. M. F. Ferreira, A. F. Martins, C. I. O. Martins, P. M. Ferreira, É. Tóth, T. B.  
4 Rodrigues, D. Calle, S. Cerdan, P. López-Larrubia, J. A. Martins and C. F. G. C.  
5 Geraldes, *Contrast Media Mol. Imaging*, 2013, **8**, 40-49.
- 6 26. M. F. Ferreira, G. Pereira, A. F. Martins, C. I. O. Martins, M. I. M. Prata, S.  
7 Petoud, E. Toth, P. M. T. Ferreira, J. A. Martins and C. F. G. C. Geraldes,  
8 *Dalton Trans.*, 2014, **43**, 3162-3173.
- 9 27. M. F. Ferreira, B. Mousavi, P. M. Ferreira, C. I. O. Martins, L. Helm, J. A.  
10 Martins and C. F. G. C. Geraldes, *Dalton Trans.*, 2012, **41**, 5472-5475.
- 11 28. S. Torres, J. A. Martins, J. P. André, C. F. G. C. Geraldes, A. E. Merbach and É.  
12 Tóth, *Chem. Eur. J.*, 2006, **12**, 940-948.
- 13 29. R. Wei, L. Cheng, M. Zheng, R. Cheng, F. Meng, C. Deng and Z. Zhong,  
14 *Biomacromolecules*, 2012, **13**, 2429-2438.
- 15 30. P. M. T. Ferreira, H. L. S. Maia, L. S. Monteiro and J. Sacramento, *J. Chem.*  
16 *Soc.-Perkin Trans. 1*, 1999, 3697-3703.
- 17 31. G. Nicolle, É. Tóth, K.-P. Eisenwiener, H. Mäcke and A. Merbach, *J Biol Inorg*  
18 *Chem*, 2002, **7**, 757-769.
- 19 32. J. P. André, É. Tóth, H. Fischer, A. Seelig, H. R. Mäcke and A. E. Merbach,  
20 *Chem. Eur. J.*, 1999, **5**, 2977-2983.
- 21 33. S. Laurent, L. Vander Elst, C. Henoumont and R. N. Muller, *Contrast Media*  
22 *Mol. Imaging*, 2010, **5**, 305-308.
- 23 34. M. Brust, M. Walker, D. Bethell, D. J. Schiffrin and R. Whyman, *Journal of the*  
24 *Chemical Society, Chem. Comm.*, 1994, 801-802.
- 25 35. A. Barge, G. Cravotto, E. Gianolio and F. Fedeli, *Contrast Media Mol. Imaging*,  
26 2006, **1**, 184-188.
- 27 36. D. M. Corsi, C. Platas-Iglesias, H. v. Bekkum and J. A. Peters, *Magn. Reson.*  
28 *Chem.*, 2001, **39**, 723-726.
- 29 37. H. Hinterwirth, S. Kappel, T. Waitz, T. Prohaska, W. Lindner and M.  
30 Lämmerhofer, *ACS Nano*, 2013, **7**, 1129-1136.
- 31 38. M.-C. Daniel and D. Astruc, *Chem. Rev.*, 2003, **104**, 293-346.
- 32 39. P. J. Krommenhoek, J. Wang, N. Hentz, A. C. Johnston-Peck, K. A. Kozek, G.  
33 Kalyuzhny, J. B. Tracy, *ACS Nano* 6 , 4903-4911.
- 34 40. M. Port, J.-M. Idée, C. Medina, C. Robic, M. Sabatou and C. Corot, *BioMetals*,  
35 2008, **21**, 469-490.
- 36 41. K. Kumar, C. A. Chang and M. F. Tweedle, *Inorganic Chemistry*, 1993, **32**,  
37 587-593.
- 38 42. A. Borel, J. F. Bean, R. B. Clarkson, L. Helm, L. Moriggi, A. D. Sherry and M.  
39 Woods, *Chem. Eur. J.*, 2008, **14**, 2658-2667.
- 40 43. F. A. Dunand, É. Tóth, R. Hollister and A. E. Merbach, *J. Biol. Inorg. Chem.*,  
41 2001, **6**, 247-255.
- 42 44. G. J. Stasiuk, S. Tamang, D. Imbert, C. Gateau, P. Reiss, P. Fries and M.  
43 Mazzanti, *Dalton Trans.*, 2013, **42**, 8197-8200.
- 44 45. S. Torres, M. I. M. Prata, A. C. Santos, J. P. André, J. A. Martins, L. Helm, É.  
45 Tóth, M. L. García-Martín, T. B. Rodrigues, P. López-Larrubia, S. Cerdán and  
46 C. F. G. C. Geraldes, *NMR in Biomed.*, 2008, **21**, 322-336.
- 47 46. N. Raghunand, C. Howison, A. D. Sherry, S. Zhang and R. J. Gillies, *Magn.*  
48 *Reson. Med.*, 2003, **49**, 249-257.
- 49 47. D. Baumann and M. Rudin, *Magn Reson Imaging*, 2000, **18**, 587-595.
- 50 48. L. Helm, *Future Medicinal Chemistry*, 2010, **2**, 385-396.

- 1 49. F. Yerly, VISUALISEUR/OPTIMISEUR, EPFL, 2003.
- 2 50. MOPAC2012, James J. P. Stewart; *Stewart Computational Chemistry*, Colorado
- 3 Springs, CO, USA, [HTTP://OpenMOPAC.net](http://OpenMOPAC.net) (2012).
- 4 51. J. P. Stewart, *J Mol Model*, 2007, **13**, 1173-1213.
- 5 52. A. Klamt and G. Schuurmann, *J. Chem. Soc., Perkin Trans. 2*, 1993, 799-805.

6

7